INTERFERENCE, OUTAGE, AND THROUGHPUT IN MOBILE WIRELESS NETWORKS

A Dissertation

Submitted to the Graduate School
of the University of Notre Dame
in Partial Fulfillment of the Requirements
for the Degree of

Doctor of Philosophy

by

Zhenhua Gong

Martin Haenggi, Director

Graduate Program in Electrical Engineering
Notre Dame, Indiana

March 2013

© Copyright by

Zhenhua Gong

2013

All Rights Reserved

INTERFERENCE, OUTAGE, AND THROUGHPUT IN MOBILE WIRELESS NETWORKS

Abstract

by

Zhenhua Gong

This dissertation characterizes the geometry of mobile wireless networks and their performance. In mobile networks, distance variations caused by node mobility generate fluctuations of the channel gains. Such fluctuations can be treated as another type of fading besides multi-path effects. Interference statistics in mobile random networks are characterized by incorporating the distance variations of mobile nodes to the channel gain fluctuations. The mean interference is calculated at the center and at the border of a finite mobile network. The network performance is evaluated in terms of the outage probability. Compared to a static network, the interference in a single snapshot does not change under uniform mobility models. However, random waypoint mobility increases (decreases) the interference at the center (at the border).

Due to the correlation of node locations (in mobile or static networks), the interference and outage are temporally and spatially correlated. We quantify the temporal correlation of the interference and outage in mobile Poisson networks in terms of the correlation coefficient of the interference and conditional outage probability, respectively. The results show that it is essential that routing, MAC scheduling, and retransmission schemes need to be smart (*i.e.*, correlation-aware) to avoid bursts of transmission failures.

For communication between two neighboring nodes in wireless networks, the local

delay, which is defined as the time it takes a node to successfully transmit a packet, is an important quantity. Previous research focuses on the local delay in static or infinitely mobile Poisson networks with ALOHA. In this dissertation, we extend the local delay results to Poisson networks with finite mobility. Bounds of the local delay in mobile Poisson networks are derived for different mobility and transmission models. Although mobility helps reduce the local delay, its impact depends on the particular mobility model. The phase transition that marks the jump of the local delay from finite to infinite is also characterized.

CONTENTS

FIGURES iv

ACKNOWLEDGMENTS vii

SYMBOLS ix

CHAPTER 1: INTRODUCTION 1
1.1 Motivation 1
1.2 Related Work 4
1.3 Organization of the Dissertation 5

CHAPTER 2: INTERFERENCE AND OUTAGE IN MOBILE RANDOM NETWORKS: SINGLE-SNAPSHOT ANALYSIS 6
2.1 Introduction 6
2.2 System model 8
2.2.1 Network model 8
2.2.2 Mobility models 9
2.2.2.1 Constrained i.i.d. mobility (CIM) 10
2.2.2.2 Random walk (RW) 12
2.2.2.3 Discrete-time Brownian motion (BM) 12
2.2.2.4 Random waypoint (RWP) 13
2.2.3 Channel access scheme 13
2.2.4 Channel model 14
2.2.5 Total interference and outage probability 15
2.3 Mean Interference 15
2.4 Single-snapshot analysis of interference and outage 20
2.4.1 Interference in uniformly mobile networks 20
2.4.2 Interference in non-uniformly mobile networks 20
2.4.2.1 Interference in finite networks without fading 20
2.4.2.2 Interference in finite networks with fading 22
2.4.2.3 Interference in infinite networks 23
2.4.3 Tightness of the outage lower bound 27
2.5 Summary 28

CHAPTER 3: INTERFERENCE AND OUTAGE IN MOBILE RANDOM NETWORKS: TEMPORAL CORRELATION . . . 30
3.1 Introduction . . . 30
3.2 Temporal correlation of interference . . . 31
3.2.1 Constrained i.i.d. mobility (CIM) . . . 36
3.2.2 Random walk (RW) . . . 41
3.2.3 Discrete-time Brownian motion (BM) . . . 41
3.3 Outage correlation . . . 42
3.4 Summary . . . 48

CHAPTER 4: THE LOCAL DELAY IN MOBILE RANDOM NETWORKS . 49
4.1 Introduction . . . 49
4.2 System model . . . 50
4.2.1 Transmitter process . . . 50
4.2.2 Transmission scheme and receiver process . . . 50
4.2.2.1 Random bipolar model . . . 52
4.2.2.2 Quasi-nearest-receiver model . . . 52
4.2.2.3 Nearest-receiver model . . . 52
4.2.3 Mobility models . . . 53
4.2.4 Local delay definition . . . 55
4.3 Local delay for deterministic transmission distance . . . 56
4.3.1 Fast mobility . . . 56
4.3.2 Block mobility . . . 61
4.4 Local delay for random static transmission distance . . . 66
4.5 Local delay for random time-variant transmission distance . . . 72
4.5.1 Random bipolar model . . . 72
4.5.2 Quasi-nearest-receiver (QNR) transmission . . . 75
4.5.3 Nearest-receiver (NR) transmission . . . 79
4.6 Conclusions . . . 81

CHAPTER 5: SUMMARY AND FUTURE WORK . . . 82
5.1 Summary of contributions . . . 82
5.1.1 Theoretical results . . . 82
5.1.2 Experimental results . . . 84
5.2 Future directions . . . 84

BIBLIOGRAPHY . . . 86

FIGURES

2.1 Illustrations of finite and infinite mobile networks. The small circles denote mobile nodes and the arrows show the directions in which they will move in the next time slot. In (a), the nodes bounce back when they reach the boundary. In (b), all nodes move freely. 9

2.2 Mobility and transmission time scales. The mobility (time) slots are indicated in (a). If a node is scheduled to transmit, each transmission period, which is presented in gray, is assumed to start at the beginning of each mobility slot. In (b), the transmission duration is much shorter than the mobility (time) slot; in (c), the length of transmission time is comparable to the mobility slot. 11

2.3 The mean interference at the origin o and at the border location z, $\|z\| = R$, under the non-singular path-loss model. 18

2.4 Simulation results versus the corresponding lower bounds of the outage probability for different fading and mobility models. 23

2.5 The outage probabilities under the RWP mobility with different radii R for the case without fading. The bound (solid curve) is obtained from (2.31). The curves with finite R are simulation results. 26

3.1 The temporal correlation coefficient ρ_1 versus the mean speed $\bar{v}$ under different mobility models. 37

3.2 The temporal correlation coefficient ρ_τ versus ϵ under the CIM model. 38

3.3 Numerical evaluation (from (3.1)) of the temporal correlation coefficient ρ_τ versus the mean node speed $\bar{v}$ with the corresponding upper bound (from (3.12)). The mobility model is CIM. 39

3.4 Numerical evaluation (from (3.1)) of the temporal correlation coefficient ρ_1 versus the mean node speed $\bar{v}$ with the corresponding upper bound (from (3.14)). The mobility model is RW. 40

3.5 The interference correlation coefficient ρ_1 versus the mean speed $\bar{v}$ under three mobility models. 43

3.6 The conditional outage probabilities $\mathbb{P}(A_t \mid A_s)$ and $\mathbb{P}\left(A_t \mid \bar{A}_s\right)$ together with the unconditional outage probability $\mathbb{P}(A_t)$ versus the threshold θ under the CIM model. The dashed curve is the unconditional outage probability; the dash-dotted curve is the upper bound of $\mathbb{P}(A_t \mid A_s)$ from (3.19); the solid-line curve is the exact expression of $\mathbb{P}(A_t \mid A_s)$ via simulations; the stars are $\mathbb{P}(A_t \mid \bar{A}_s)$ via simulations; the $\times$ is the lower bound of $\mathbb{P}\left(A_t \mid \bar{A}_s\right)$ from (3.21). 46

3.7 The conditional outage probabilities $\mathbb{P}(A_t \mid A_s)$ and $\mathbb{P}\left(A_t \mid \bar{A}_s\right)$ together with the unconditional outage probability $\mathbb{P}(A_t)$ versus the MAC scheme parameter p under the CIM model. 47

4.1 Three types of transmission models. The triangles and crosses represent receivers and transmitters, respectively. The potential transmitter receiver pairs are connected by dashed lines. The transmitters are mobile in a circular region of radius $a_0 = 1$. The dotted circles represent their mobility regions. The network intensity $\lambda_0 = 0.1$. Under the random bipolar scheme (a), each transmitter has an assigned receiver, whose location is at the home location of the transmitter. Under quasi-nearest-receiver (b) and nearest-receiver (c) schemes, the receiver process, whose intensity is $\lambda' = 0.07$, is independent of the transmitter process. In (b), the assigned receiver is not always the nearest receiver to the transmitter, and the transmitter keeps transmitting to the same receiver. In (c), however, the transmitter always transmits to its nearest receiver. 51

4.2 The conditional local delay $D_v(\theta \mid R)$ as a function of the mean speed $\bar{v}$ under UM and NM. $\bar{v} = 128a_0/45\pi$ for UM and $\bar{v} = \sqrt{\pi}\sigma$ for NM. The simulation result is the solid curve. The dashed curve is an upper bound from (4.11). The dotted line is the infinitely mobile case, which provides a lower bound. The static case ($v = 0$) is represented in a triangle. 62

4.3 The conditional local delay $D_K(\theta \mid R)$ as a function of the mean location coherence time K under UM and NM. The simulation and an upper bound from (4.19) are marked by circles and solid curve, respectively. The dashed line is the static case. 65

4.4 The local delay as a function of the mean transmission distance $\bar{R} = \mathbb{E}[R]$, where $a_0 = 45\pi\bar{R}/128$ and $\sigma = \bar{R}/\sqrt{\pi}$. The solid curve shows the simulation results for fast mobility only at interferers with their upper and lower bounds in circles and dashed lines, respectively. The crosses are the static case. 73

4.5 Local delay under the random bipolar model for UM and NM. For comparison, the conditional local delay for a fixed transmission distance $R = 15\pi\bar{v}/64$ is also included, where the upper bound is from (4.11) with $R = 15\pi\bar{v}/64$. 76

4.6 The local delay as a function of the transmission probability p under quasi-nearest-receiver and nearest-receiver transmission schemes. The crosses and circles are the simulation results of QNR and NR schemes, respectively. The dotted line is an upper bound of the local delay under the QNR scheme (see (4.32) and (4.33)). The dashed line is the static case. The solid curve is a lower bound of the local delay under the QNR scheme (see (4.30)). 80

ACKNOWLEDGMENTS

First of all, I thank my advisor Professor Martin Haenggi for his support, supervision, and encouragement throughout my doctoral studies at the University of Notre Dame. I benefit a lot from his rigor and perfection in research work. He made my research and studies enjoyable and rewarding experience.

I thank the faculties and staffs in Electrical Engineering for their teaching and work. I appreciate Professor Fuja, Laneman, Minero, and Bauer for their time to be the committees of my candidacy and doctoral defenses. The discussion with them is very beneficial.

I thank fellow graduate students and scholars Xinchen Zhang, Zhanwei Sun, Peter Vizi, Chia-Han Lee, Sunil Srinivasa, Radha Ganti, Sundar Vanka, Wangqing Yuan, Po Wu, Guowang Li, Lai Wei, Yuzhe Liu, Zhen Tong, and Anjin Guo - to name a few - in the department for their friendship and inspiring technical discussions. It is because these fellow students and scholars that make my life in South Bend and pursuing the Ph.D. degree much easier. I thank Professor Yu-Chi Chang and Mrs Priscilla Wong for their support to student activities and make Notre Dame as home to me.

I also thank my parents Shangjun Gong and Jianzhong Chen for their self-giving support and constant encouragement. Their support is throughout my life: from early age to secondary school, to college, and to Notre Dame. Their leadership affact me a lot in my life and studies. I love them. I thank my aunt Jianqing Chen for her help during my first year coming to the United States. I also appreciate my grandparents and other relatives for their kind encouragement.

Last but not least, I thank P3 Communications Inc. and Research In Motion Ltd. for their excellent summer internship programs. The internship experience not only provided me an opportunity to work in wireless industry but also helped my research back at Notre Dame. The internship also helped in expanding my understanding in wireless communications and networking, and in building the bridge for me between the academic research and industry applications.

SYMBOLS

A_t	The event that the link is in outage at time t
$B(o, R)$	Disk center at o with radius R
D	Local delay in the number of time slots
d	Network dimension
$d_{\mathcal{H}}$	Hausdorff dimension
$g(x)$	$\triangleq \frac{1}{\epsilon+\|x\|^{\alpha}}$ large-scale path-loss function
h	Multi-path fading gain
$I(t)$	Total interference at time t
I_1	Interference from the nearest interferer
K	Average location coherence time
o	The origin
p	ALOHA MAC transmission probability
q	$\triangleq 1 - p$
p_{o}	Outage probability
R_1	Distance between a node and its nearest neighbor
R_{CIM}	$\triangleq 45\pi/128$, normalized mobility range of constraint i.i.d. mobility model
R_{RW}	$\triangleq 1.5$, normalized mobility range of random walk model in one time slot
$\mathcal{S}$	Static elements of a network
$\mathcal{C}_{\mathcal{S}}$	The event that a single transmission is successful conditioned on $\mathcal{S}$
t	Time measured in slots
$v_i(t)$	Speed of node i at time t
$\bar{v}$	$\triangleq \mathbb{E}[v_i(t)]$, mean speed

α	Path loss exponent
β	$\triangleq \sqrt{(1-q^{1-\delta})\pi/p\gamma}$
δ	$\triangleq d/\alpha$
θ	Outage threshold
λ_0	Node intensity
λ'	$= q\lambda_0$ receiver intensity
γ	$\triangleq \delta\pi^2\theta^\delta/\sin(\pi\delta)$, the spatial contention
τ	Time difference
ρ_τ	Temporal correlation coefficient of the interference
$\Phi(t)$	$\triangleq \{x_i(t)\}$, the transmitter process
$\tilde{\Phi}$	$\triangleq \{y_i\}$ the home location process of the transmitters
Ψ	The receiver process
$\mathcal{L}_I(s)$	Laplace transform of the interference

CHAPTER 1

INTRODUCTION

1.1 Motivation

There are two fundamental aspects of wireless networks that make the design and analysis challenging and interesting. First is the phenomenon of fading: the time variation of the channel strengths due to small-scale effects (multi-path fading), as well as large-scale effects (path-loss) via distance attenuation, and shadowing by obstacles. Second, unlike in the wired world where each transmitter-receiver pair can usually be thought of as an isolated point-to-point link, wireless nodes communicate over the air and share common resources. The competition among different users is thus severe, since the resources are limited. The interference can be between different transmitter-receiver pairs, between transmitters communicating with a common receiver, or between signals from a single transmitter to multiple receivers. Hence, fading and interference are two central elements we need to consider in the network performance analysis [1].

There are four major sources of randomness that affect the interference in large networks. The first element is fading, which has been described previously. The second one is node placement. In mobile networks, a random model of spatial locations is necessary to facilitate the network analysis. A well-accepted model for the node distribution in wireless networks is the homogeneous Poisson point process (PPP) [2, 3, 4], where the number of nodes in a certain region of area A is Poisson distributed with parameter $\lambda_0 A$, where λ_0 is defined as node intensity. The numbers

of nodes in disjoint regions are mutually independent. The third one is data traffic. In cellular networks, for example, base stations schedule the data transmission to reduce the interference. On the other hand in distributed medium access control (MAC) protocols, ALOHA [5, 6, 7] and CSMA [8, 9, 10] are two classes of well-accepted protocols. The fourth one is transmit power. Power control helps in the management of interference (ensuring efficient spectral reuse and desirable user experience), energy optimization (minimizing overall energy expense), and connectivity (maintaining logical connectivity) [11, 12, 13]. When power control is implemented locally, the receiver is not aware of the power levels of other, interfering transmitters, the power levels hence become a source of randomness in wireless networks.

For the sake of mathematical tractability and simplicity, the above four sources of randomness are often assumed identically and independently distributed (i.i.d.). For example, the channels are often assumed to be memoryless; if mobility is at all considered, the nodes in a network are infinitely mobile so that the realizations of node locations are independent in different time slots; the node activities are not affected by previous activities. Are those assumptions realistic? In wireless networks, the i.i.d. assumptions for multi-path channel realizations, transmit power levels, and data traffic statistics are reasonable, if nodes transmit in short bursts. Furthermore, some broadband transmission techniques, such as frequency-hopping spread-spectrum, nullify the channel memories as well. For node placement, however, the situation is different. The correlation between node locations in different time slots is zero only if a completely new realization of the node placement is drawn in each time slot. Network models assuming independent realizations are impractical since the node velocities cannot be infinite. If the node placement follows a certain type of distribution such as a PPP in each time slot and the nodes do not have infinite mobility, the node locations in different time slots are correlated. An extreme case is the static but random network, where the nodes' positions are completely correlated,

since the nodes do not move after their initial placement.

How does mobility affect network structure and performance? First, it is well known that multi-path fading is induced by *microscopic* mobility. A slight position change of a node induces the randomness in channel gain. On the other hand, when distance is considered in a wireless transmission, a significant change in the transmission distance, which is called *macroscopic* mobility, gives rise to another degree of uncertainty: path-loss uncertainty. We denote the multi-path fading simply as *fading* and large-scale path-loss uncertainty as *large-scale fading*. Both types of fading are induced by mobility. Second, mobility affects temporal and spatial correlation. The locations of a node always show a certain degree of correlation in different time slots, since the node speed is finite. The quantification of such correlation is worthwhile. Third, mobility induces spatial diversity. Due to the nature of multi-path fading, a node observes multiple uncorrelated channel realizations in mobile environment. Deep fading locations can thus be avoided.

It is fundamentally necessary that every node is able to successfully transmit messages to at least one other node in the network in a finite amount of time. Hence, the local delay, which is defined in [14, 15] as the average time (in numbers of time slots) until a packet is successfully transmitted, is an important quantity. The local delay and its phase transition condition in static Poisson networks are analyzed in [14]. The local delay in power- and interference-limited networks is presented in [15]. Only two extreme cases are considered in their analysis: the network is either completely static (nodes do not move after initial placement), or infinitely mobile (a new and independent Poisson point process (PPP) is drawn in each time slot). However, no work has analyzed the local delay under practical (finite) mobility models, which is the important intermediate regime between the two extreme cases.

1.2 Related Work

There is a growing body of literature of large wireless networks with randomly distributed nodes. Stochastic geometry [2, 4] and the theory of random geometric graphs [16] are two increasingly widely used analysis tools. Interference and outage statistics are obtained in the case where nodes are Poisson distributed without multi-path fading [17, 18] and in the presence of fading [19, 20]. For the node placement models other than homogeneous Poisson, distance statistics in finite uniformly random networks are obtained in [21]. Interference and outage in clustered ad hoc networks are discussed in [22]. Interference results for ad hoc networks with general motion-invariant node distribution are presented in [23, 24, 25]. The interference distribution in doubly Poisson cognitive networks is analyzed in [26]. In [27], the hardcore point process is approximated by a non-homogeneous PPP to evaluate the outage. The performance of spatial relay networks is analyzed in [28, 29]. Routing in ad hoc networks is discussed in [19, 30, 31, 32]. The throughput and capacity in interference-limited networks have been derived in [33, 34, 35]. The spatio-temporal correlation of the interference and outage in static random networks has been studied in [36]. The spatial distribution of link outages in static random networks has been derived in [37]. The temporal correlation properties of the interference in static networks has been discussed in [38] in terms of the node locations, Rayleigh block fading, and traffic. In [39], the interference correlation is shown to induce diversity loss in Poisson neworks with multi-antenna receivers.

Related work on mobile networks includes [40], where a network of mobile nodes is mapped to a network of stationary nodes with dynamic links. Mobility is shown to increase the capacity of ad hoc networks by exploiting multi-user diversity [41]. In [42], different mobility models and their effects to ad hoc networks are compared. The stochastic properties of random walk and random waypoint mobility models are analyzed in [43] and [44, 45, 46, 47], respectively. Another way of combining

micro- and macroscopic path loss uncertainty has been explored in [48], where small-scale fading is interpreted as a distortion of the point process in modeling the node locations.

Besides the local delay analysis in static and infinitely mobile Poisson networks [14, 15], the local delay in clustered networks is analyzed in [49]. A set of power control policies are provided in [13] to minimize the local delay in static Poisson networks. The interference correlation due to long transmission duration and the corresponding local delay are evaluated in [50] using joint interference statistics. The throughput/delay and power/delay tradeoffs for mobile ad hoc networks have been evaluated in [51, 52] and [53], respectively. A delay analysis for two-hop relay networks is presented in [54]. The delay in buffered ALOHA networks has been analytically characterized in [55].

1.3 Organization of the Dissertation

In this dissertation, we present the analysis of mobile wireless networks from theoretical perspective. In Chapters 2 and 3, we analyze the interference and outage in mobile random networks. We start with single-snapshot analysis of interference and outage in Chapter 2. The temporal correlation of the interference and outage is analyzed in Chapter 3. We calculate the correlation coefficient of the interference and the conditional outage probability. The contents in Chapter 2 and 3 form [56]. In Chapter 4, the local delay in mobile Poisson networks is analyzed and conrete results of either exact expressions or bounds are obtained. The content of Chapter 4 forms [57]. Chapter 5 summarizes the contributions and discusses several future directions.

CHAPTER 2

INTERFERENCE AND OUTAGE IN MOBILE RANDOM NETWORKS: SINGLE-SNAPSHOT ANALYSIS

2.1 Introduction

Multi-path fading models, *e.g.*, the Rayleigh and Nakagami models, have been frequently employed to characterize wireless channels, treating small-scale fading, which is induced by microscopic mobility, as a stochastic component. On the other hand, power decay with distance or large-scale path loss is typically modeled as a deterministic component, given that the locations of a transmitter and a receiver are known or that the location uncertainty compared to the transmission distance is negligible. However, macroscopic mobility, which generates macroscopic changes in the transmission distance, also induces fluctuations of the channel gains. Hence, it can be viewed as another source of fading (path-loss uncertainty) in wireless environments, in addition to the multi-path effects. To make the definitions clear, we define the channel as

$$G \triangleq h \cdot g(x), \tag{2.1}$$

where h is the multi-path fading and $g(x)$ is the path loss function.

Understanding the large-scale fading induced by macroscopic mobility is essential to deal with random networks because nodes are mobile in many applications. In [40], a network of mobile nodes is mapped to a network of stationary nodes with dynamic links. Path loss and fading uncertainties are treated jointly for single-hop connectivity and broadcasting in [48]. Previous research has only considered the

distance uncertainty in the analysis. Interference in mobile networks remains an open problem. However, interference is one of the main issues in wireless networks, since it often limits network performance [1]. Closed-form results for the interference and signal-to-interference ratio (SIR) distributions in static random networks are available in [12, 17, 19]. To the best of our knowledge, no work has focused on the interference statistics in mobile random networks.

In this chapter, we characterize the interference distribution in mobile networks. Several well-accepted mobility models are considered in the analysis. The outage probability is used as a performance metric. In order to get closed-form expressions of the interference distribution and the outage probability, we approximate the total interference by only considering the contribution of the nearest interferer to a receiver.

To illustrate how macroscopic mobility and large-scale fading are related, we start with a simple motivating example. The received power is exponentially distributed, if the channel is subject to the Rayleigh fading. As a consequence, the SNR is exponential, as well as the SIR for constant interference power I. Next, we consider an infinite Poisson network with node intensity λ_0. Nodes are infinitely mobile, which means that a new realization of the homogeneous PPP is drawn in every time slot. At a receiver, if we only focus on the interference from its nearest neighbor, the SIR $\eta = 1/I = R_1^{\alpha}$, where R_1 is the distance between the receiver and its nearest neighbor, and α is the path loss exponent. From [48], we have the pdf of R_1 as

$$f_{R_1}(r) = 2\lambda_0 \pi r e^{-\lambda_0 \pi r^2}, \qquad r \geqslant 0. \tag{2.2}$$

Evidently, the pdf of η is given by

$$f_{\eta}(x) = \delta \lambda_0 \pi x^{\delta - 1} e^{-\lambda_0 \pi x^{\delta}}, \qquad x \geqslant 0, \tag{2.3}$$

where $\delta \triangleq 2/\alpha$. η follows a Weibull distribution. For $\delta = 1$, we obtain

$$f_\eta(x) = \lambda_0 \pi e^{-\lambda_0 \pi x}, \tag{2.4}$$

which is an exponential distribution. Hence, the distance variation leads the receiver to have the same SIR distribution as in the Rayleigh fading case! In other words, the receiver observes fading effects through the wireless channels due to the macroscopic mobility. It can be treated as another source of dynamics. In this example, the fading is more severe, when $\delta < 1$. Based on this observation, we characterize the interference distribution in mobile networks by mapping the distance variations of mobile nodes to the received power fluctuations in wireless channels.

The rest of the chapter is organized as follows. System and mobility models are introduced in Section 2.2. In Section 2.3, the mean interference at the center and at the border of a finite mobile network is calculated. The single-snapshot analysis of the interference and outage in mobile random networks is discussed in Section 2.4. Section 2.5 concludes the chapter.

2.2 System model

2.2.1 Network model

We consider the link between a transmitter-receiver pair in a wireless network with the receiver at the origin o. Without loss of generality, the link distance is normalized to one (equivalently, we can say that the path-loss component is compensated for in the desired link). Other potential interferers are randomly distributed[1]. The initial node placement follows a PPP $\tilde{\Phi}$ on a domain $\mathbb{D} \subseteq \mathbb{R}^2$ with intensity λ_0. In a finite network as shown in Fig. 2.1 (left), $\mathbb{D} = B(o, R)$, where $B(o, R)$ is a disk of radius

[1]We do not consider the assigned receivers of interfering transmitters, since they do not affect the network geometry in our analysis.

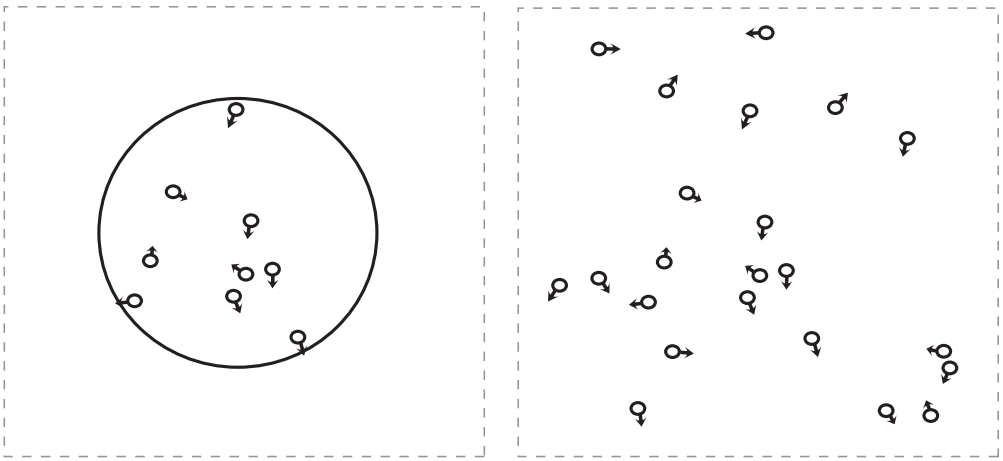

(a) Finite network (b) Infinite network

Figure 2.1. Illustrations of finite and infinite mobile networks. The small circles denote mobile nodes and the arrows show the directions in which they will move in the next time slot. In (a), the nodes bounce back when they reach the boundary. In (b), all nodes move freely.

R centered at o. The number of nodes M inside $B(o, R)$ is Poisson distributed with mean $\lambda_0 \pi R^2$. In an infinite network as shown in Fig. 2.1 (right), $\mathbb{D} = \mathbb{R}^2$.

The nodes move independently of each other by updating their positions at the beginning of each time slot. In a finite network, nodes bounce back when they reach the boundary so that M remains constant. In an infinite network, all nodes move freely. In both cases, the locations of potential interferers follow a homogeneous or non-homogeneous PPP $\Phi(t) = \{x_i(t)\}$ at any time $t \in \mathbb{N}$.

2.2.2 Mobility models

Different mobility models lead to different spatial properties of the networks and, in turn, affect the network performance differently [42]. In this part, we introduce several well-accepted models. For a fair comparison between different models, we first define the average speed of the nodes and set it to the same level. The speed of node i in one time slot is defined as $v_i(t) = \|x_i(t) - x_i(t-1)\|$, where $t \in \mathbb{N}$ and $\|\cdot\|$

is the Euclidean distance. We define $v_i(t) \triangleq \|x_i(t) - x_i(t-1)\|$. Let

$$\bar{v}_i(t) \triangleq \mathbb{E}\left[v_i(t)\right], \qquad \forall t \in \mathbb{Z}.$$

Due to ergodicity and point process homogeneity, the mean speed averaged over all nodes for a fixed time t is equal to the mean speed averaged over time for a fixed node. Hence, we drop i and t, and simply denote by $\bar{v}$ the mean speed of the node. The time slot is measured at the time scale of mobility, which is indicated Fig. 2.2(a). The mean distance that a node travels in one time slot is assumed larger than the radio signal wavelength. The communication time scale, which will be introduced in the next sub-section, is much shorter or at the level of the mobility (see Fig. 2.2(b) and 2.2(c)).

2.2.2.1 Constrained i.i.d. mobility (CIM)

The CIM model is first introduced in [40]. Here, we consider an identical model except for the first time slot at $t = 0$. The node location $x_i(t)$ is

$$x_i(t) = y_i + \bar{v} w_i(t), \tag{2.5}$$

where the home locations of the nodes are $\tilde{\Phi} = \{y_i\}$; $w_i(t)$ is uniformly at random in $B(y_i, \bar{v}R_{\text{CIM}})$. Using the results from [47], we calculate the normalized mobility range[2] $R_{\text{CIM}} = 45\pi/128 \approx 1.1045$. The CIM model is non-Markov. However conditioning on y_i, we have $x_i(t)$ and $x_i(t+s)$ are i.i.d. for all $t, s > 0$.

[2]The term "normalized" means that the average node speed is equal to one.

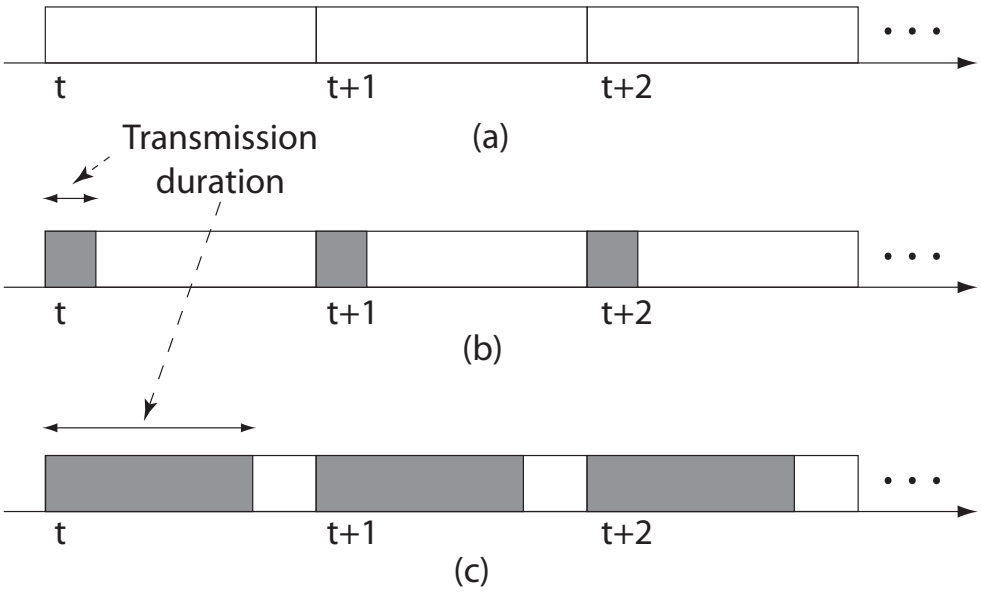

Figure 2.2. Mobility and transmission time scales. The mobility (time) slots are indicated in (a). If a node is scheduled to transmit, each transmission period, which is presented in gray, is assumed to start at the beginning of each mobility slot. In (b), the transmission duration is much shorter than the mobility (time) slot; in (c), the length of transmission time is comparable to the mobility slot.

2.2.2.2 Random walk (RW)

Under the RW model, a mobile node selects a new direction and speed randomly and independently in each time slot. Hence, the spatial node distribution remains uniform [43]. Mathematically, the location of node i at time $t+1$ for $t \in \mathbb{N}$ is

$$x_i(t+1) = x_i(t) + \bar{v} w_i(t), \tag{2.6}$$

where the distribution of $w_i(t)$ is uniformly at random in $B(x_i(t), \bar{v} R_{\mathrm{RW}})$. The normalized mobility range $R_{\mathrm{RW}} = 1.5$, which is straightforward.

2.2.2.3 Discrete-time Brownian motion (BM)

Under the discrete-time BM model, the node location at time $t+1$ for $t \in \mathbb{N}$ is

$$x_i(t+1) = x_i(t) + \bar{v} w_i(t), \tag{2.7}$$

where $w_i(t) = [w_{i,1}(t), w_{i,2}(t)]^T$ and $w_{i,1}(t)$ and $w_{i,2}(t)$ are i.i.d. normally distributed *i.e.*, $w_{i,1}(t), w_{i,2}(t) \sim \mathcal{N}(0, \sigma_1^2)$. After normalization, we have $\sigma_1 = \sqrt{2/\pi}$.

Remark. From [19], [43, Lemma 2.2], and [58], the above mobility models with the bouncing behavior in a finite network[3] preserve the uniform properties of the node distribution. Consequently for any t, if the initial PPP is homogeneous, the PPP $\Phi(t)$ remains homogeneous. We categorize CIM, RW, and BM models as uniform mobility models (UMM).

[3] A more detailed discussion on the border behavior and effects in mobile networks is presented in [44].

2.2.2.4 Random waypoint (RWP)

This model is only strictly defined in a finite region. Each node uniformly chooses a destination in the region and moves towards it with randomly selected speed[4]. A new direction and speed are chosen only after the node reaches the destination. Otherwise, it keeps the same direction and speed for several time slots. The steady-state node distribution is a *non-uniform* distribution [45]. We denote the distance of a typical node to the origin at steady state by L. For $\mathbb{D} = B(o, R)$, the probability density function (pdf) of L is given by

$$f_L(r) = \frac{1}{R^2}\left(-\frac{4r^3}{R^2} + 4r\right). \tag{2.8}$$

The intensity measure of the point process follows as

$$\Lambda(B(o,r)) \triangleq \mathbb{E}(\Phi(B(o,r))) = 2\lambda_0\pi r^2 - \frac{\lambda_0\pi r^4}{R^2},$$

where $r \leqslant R$. The intensity function is thus given by

$$\lambda(x) \triangleq \lambda_\infty(x) = 2\lambda_0 - \frac{2\lambda_0 \left\|x\right\|^2}{R^2}. \tag{2.9}$$

2.2.3 Channel access scheme

We assume that transmissions start at the beginning of each time slot and that each transmission is finished within one time slot as shown in Fig. 2.2(b) and 2.2(c). The next transmission (if the node is scheduled to transmit) starts at the beginning of the next mobility (time) slot. Slotted ALOHA is assumed as the MAC protocol. In every time slot t, each node determines whether to transmit or not independently with probability p. This channel access scheme minimizes the correlation. Note that the

[4]In the simulations, the speed is chosen so that the travel distance is a multiple of the speed.

model is also suitable for the case where not all transmissions start at the beginning of a mobility time slot, since spreading out the transmissions using time division scheduling reduces the density of interferers. This case is modeled by reducing the transmit probability p by an appropriate factor.

2.2.4 Channel model

The attenuation in the wireless channel is modeled as the product of a large-scale path-loss component and a small-scale fading component. The path-loss function $g(x)$ is given by

$$g(x) = \frac{1}{\epsilon + \|x\|^{\alpha}}, \qquad \epsilon \geqslant 0, \tag{2.10}$$

where α is the path loss exponent. Two categories of models are usually considered: the singular path-loss model where $\epsilon = 0$ and the non-singular path-loss model where $\epsilon > 0$. $rg(r) = r/\left(\epsilon + r^{\alpha}\right)$ is assumed to be integrable, *i.e.*,

$$\int_{\nu}^{\infty} rg(r)\mathrm{d}r < \infty, \qquad \forall \nu > 0.$$

$\alpha > 2$ is necessary and sufficient to satisfy the integrability condition.

For the multi-path fading, we consider a deterministic model (*i.e.,* no fading) and the Rayleigh and Nakagami fading models in the desired link and the interfering links. In Rayleigh fading, the pdf of the power fading gain h is given by

$$f_h(x) = \exp(-x).$$

In the more general Nakagami-m fading model, the pdf of the power fading gain is given by

$$f_h(x) = \frac{m^m x^{m-1} \exp(-mx)}{\Gamma(m)}, \qquad m > 0.$$

If the transmission duration is relatively long, *i.e.*, comparable to the length of

the mobility (time) slot (Fig. 2.2(c)), the packet may observe a large number of realizations, since the node covers many wavelengths in distance. With interleaving, the fading will then have a negligible effect corresponding to a large m or even $m \to \infty$ (no fading). If the transmissions are short (Fig. 2.2(b)), on the other hand, fading needs to be accounted for using the Rayleigh or Nakagami models with small m.

2.2.5 Total interference and outage probability

At time t, the total interference at the receiver (located at z) is given by

$$I(t) = \sum_{x \in \Phi(t)} T_x(t) h_x(t) g(x - z), \tag{2.11}$$

where the random variables $T_x(t)$ are i.i.d. Bernoulli with parameter p due to ALOHA; $h_x(t)$ is the multi-path fading with mean $\mathbb{E}h = 1$. The family of random variables $I(t)$, $t \in \mathbb{Z}$, are exchangeable [59].

The outage probability $p_{\rm o}$ is one of the fundamental performance metrics in wireless networks. In interference-limited channels, an outage occurs if the signal-to-interference ratio (SIR) at a receiver is lower than a certain threshold θ *i.e.*,

$$p_{\rm o} \triangleq \mathbb{P}(\text{SIR} < \theta). \tag{2.12}$$

2.3 Mean Interference

In this section, we calculate the mean interference in a network under either UMM or RWP mobility. For $\epsilon > 0$ and $\alpha = 4$, it is known [12] that the mean interference at the origin under UMM is given by

$$\mathbb{E}[I_{o,\text{UMM}}] = \frac{\pi p \lambda_0}{\sqrt{\epsilon}} \arctan \frac{R^2}{\sqrt{\epsilon}}. \tag{2.13}$$

We have the following proposition about the mean interference at the origin under the RWP model.

Proposition 2.1. *For $\alpha = 4$, a finite network of radius R, and ALOHA with parameter p, The mean interference at the origin under the RWP model is given by*

$$\mathbb{E}[I_{o,\mathrm{RWP}}] = \frac{2\pi p\lambda_0}{\sqrt{\epsilon}} \arctan \frac{R^2}{\sqrt{\epsilon}} - \frac{p\lambda_0\pi}{R^2} \ln\left(1 + \frac{R^4}{\epsilon}\right). \tag{2.14}$$

As $R \to \infty$,

$$\mathbb{E}[I_{o,\mathrm{RWP}}] \lesssim 2\mathbb{E}[I_{o,\mathrm{UMM}}], \tag{2.15}$$

where "$\lesssim$" denotes an upper bound with asymptotic equality.

Proof. Under the RWP model, we have from Campbell's theorem

$$\mathbb{E}[I_{o,\mathrm{RWP}}] = 4\pi p\lambda_0 \int_0^R \left(\frac{r}{\epsilon + r^4} - \frac{r^3}{\epsilon + r^4}\right) \mathrm{d}r.$$

The rest of the calculation is straightforward. □

For $\epsilon = 0$, we ignore the interfering nodes which are very close to the origin by setting a guard zone[5] $B(0, \nu)$, for any $\nu > 0$. We have the following proposition about the mean interference at the origin.

Proposition 2.2. *For a finite network of radius R and ALOHA parameter p, the mean interference at the origin under UMM is given by*

$$\mathbb{E}[I_{o,\mathrm{UMM}}] = \frac{2p\lambda_0\pi}{\alpha - 2} \left(\nu^{-\alpha+2} - R^{-\alpha+2}\right), \tag{2.16}$$

where ν is the guard radius in the singular path-loss model. For $\alpha = 4$, the mean

[5]The guard zone is set to keep the mean interference finite.

interference at the origin under the RWP model is given by

$$\mathbb{E}[I_{o,\mathrm{RWP}}] = 2p\lambda_0\pi\left(\nu^{-2} - R^{-2}\right) - \frac{4p\lambda_0\pi}{R^2}\ln\frac{R}{\nu}. \tag{2.17}$$

For $\alpha \neq 4$, we have

$$\begin{aligned}\mathbb{E}[I_{o,\mathrm{RWP}}] &= \frac{4p\lambda_0\pi}{\alpha-2}\left(\frac{1}{\nu^{\alpha-2}} - \frac{1}{R^{\alpha-2}}\right) \\ &\quad -\frac{4p\lambda_0\pi}{(\alpha-4)}\left(\frac{1}{\nu^{\alpha-4}R^2} - \frac{1}{R^{\alpha-2}}\right).\end{aligned} \tag{2.18}$$

As $R \to \infty$, we obtain again,

$$\mathbb{E}[I_{o,\mathrm{RWP}}] \lesssim 2\mathbb{E}[I_{o,\mathrm{UMM}}].$$

Proof. Under UMM,

$$\mathbb{E}[I_{o,\mathrm{UMM}}] = 2\pi p\lambda_0 \int_\nu^R r^{-\alpha+1}\mathrm{d}r.$$

and under the RWP model,

$$\mathbb{E}[I_{o,\mathrm{RWP}}] = 4\pi p\lambda_0 \int_\nu^R r^{-\alpha+1} - \frac{r^{-\alpha+3}}{R^2}\mathrm{d}r.$$

The rest of the calculation is straightforward. □

From Proposition 2.1 and 2.2, we find that the mean interference at the origin under the RWP model is asymptotically twice the mean interference under UMM when the radius R grows large.

Next we evaluate the mean interference at the border of a network (*i.e.*, at any z with $\|z\| = R$). For UMM, we have the following proposition.

Proposition 2.3. *For $\alpha = 4$, a finite network of radius R, and ALOHA parameter*

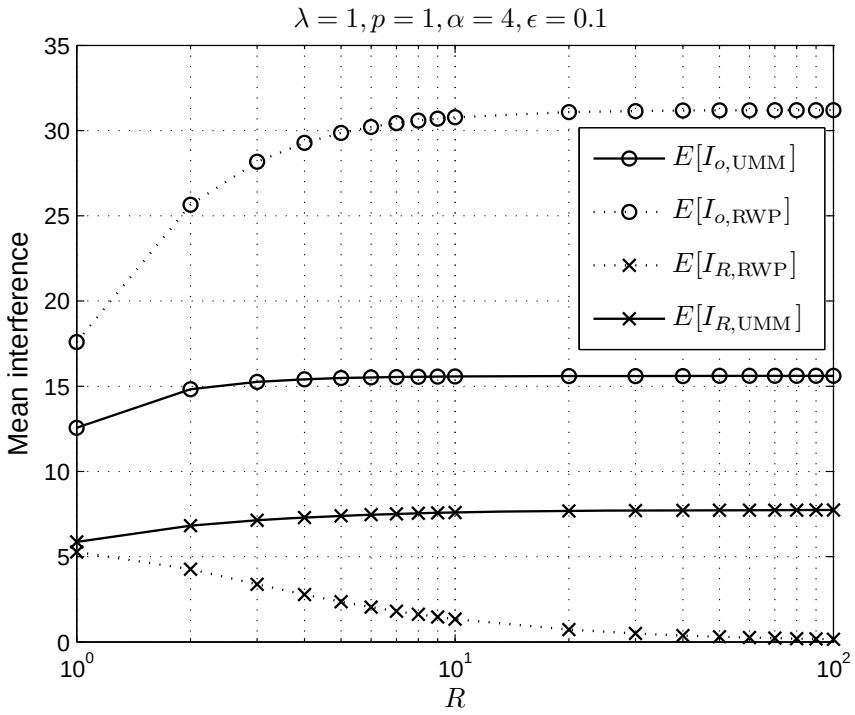

Figure 2.3. The mean interference at the origin o and at the border location z, $\|z\| = R$, under the non-singular path-loss model.

p, the mean interference at a border location z with $\|z\| = R$ under UMM is given by

$$\mathbb{E}[I_{R,\mathrm{UMM}}] = \frac{p\lambda_0}{\sqrt{\epsilon}} \int_0^1 \frac{\arctan \frac{4R^2}{\sqrt{\epsilon}} x^2}{\sqrt{1-x^2}} \mathrm{d}x, \qquad \epsilon > 0. \tag{2.19}$$

When $R \to \infty$, we have

$$\lim_{R\to\infty} \mathbb{E}[I_{R,\mathrm{UMM}}] = \frac{p\lambda_0 \pi^2}{4\sqrt{\epsilon}}, \qquad \epsilon > 0. \tag{2.20}$$

Under the RWP model, we have

$$\lim_{R\to\infty} \mathbb{E}[I_{R,\mathrm{RWP}}] = 0. \tag{2.21}$$

Proof. We have

$$\begin{aligned} \mathbb{E}[I_{R,\mathrm{UMM}}] &= p\lambda_0 \int_{B((R,0),R)} g(x)\mathrm{d}x \\ &= p\lambda_0 \int_{-\pi/2}^{\pi/2} \int_0^{2R\cos\theta} r g(r) \mathrm{d}r\mathrm{d}\theta, \end{aligned}$$

which equals (2.19). For the RWP model, the mean interference at the border is given by

$$\begin{aligned} \mathbb{E}[I_{R,\mathrm{RWP}}] &= p \int_{B(0,R)} \lambda(x) g(x-z) \mathrm{d}x \\ &= \frac{2p\lambda_0}{R^2} \int_{-\pi/2}^{\pi/2} \int_0^{2R\cos\theta} \frac{2Rr^2\cos\theta - r^3}{\epsilon + r^\alpha} \mathrm{d}r\mathrm{d}\theta. \end{aligned}$$

Letting $R \to \infty$, we obtain (2.21). □

The following corollary follows from (2.13) and (2.20).

Corollary 2.4. *Assume UMM, $\alpha = 4$, and a finite network of radius R. When*

$R \to \infty$,

$$\mathbb{E}[I_{R,\mathrm{UMM}}] \lesssim \frac{1}{2}\mathbb{E}[I_{o,\mathrm{UMM}}]. \tag{2.22}$$

Fig. 2.3 shows the mean interference at the origin o and at the border under the non-singular path-loss model. Both UMM and RWP model are considered. $\mathbb{E}[I_{R,\mathrm{RWP}}]$ decreases with R since the node intensity at the border decreases with increasing R.

2.4 Single-snapshot analysis of interference and outage

In this section, we evaluate the network performance in a single snapshot. We assume that $\epsilon = 0$. The mobility models in Section 2.2.2 are separated into two categories: uniform and non-uniform.

2.4.1 Interference in uniformly mobile networks

Because of the uniformity of the mobility, the mobile network in any time t can be treated as a correlated realization of a static network. Hence the existing results of the interference and outage in static networks in [12, 17] also apply to uniformly mobile networks.

2.4.2 Interference in non-uniformly mobile networks

2.4.2.1 Interference in finite networks without fading

We consider RWP and set $\mathbb{D} = B(o, R)$. We evaluate the interference at the origin o, since the interferer density decreases with the distance to the origin o (see (2.9)), which leads to a lower bound of the network performance. As we are only interested in the interference distribution in a single time slot, we can drop the dependence on t and focus on the generic random variable

$$I = \sum_{x \in \Phi} T_x \left\| x \right\|^{-\alpha}. \tag{2.23}$$

There is no closed-form expression for the pdf of the interference in most cases. However, since the received power decays according to a power law, only considering the interference from the nearest interferer to the receiver provides a good approximation, if the path-loss exponent α is not too close to 2 [12]. Therefore, the interference power is approximately

$$I \approx I_1 = R_1^{-\alpha}, \tag{2.24}$$

where R_1 is the distance between the origin to its nearest interferer. Given a total number of nodes M, we have

$$\begin{aligned} \mathbb{P}\left(R_1 \leqslant r \mid M\right) &= 1 - \left(1 - F_L(r)\right)^M \\ &= 1 - \left(1 - \left(\frac{2r^2}{R^2} - \frac{r^4}{R^4}\right)\right)^M, \end{aligned}$$

where $F_L(r) = \int_0^r f_L(x)\mathrm{d}x$ and $f_L(x)$ is given in (2.8). Since M is Poisson distributed with mean $p\lambda_0\pi R^2$, the pdf of R_1 is thus given by

$$\begin{aligned} f_{R_1}(r) &= \frac{\mathrm{d}\mathbb{E}_M\left[\mathbb{P}\left(R_1 \leqslant r \mid M\right)\right]}{\mathrm{d}r} \\ &= p\lambda_0\pi\left(4r - 4\frac{r^3}{R^2}\right) e^{-p\lambda_0\pi\left(2r^2 - \frac{r^4}{R^2}\right)}. \end{aligned} \tag{2.25}$$

From (2.24) and (2.25), we obtain the pdf of I_1:

$$f_{I_1}(x) = 2p\lambda_0\pi\delta\left(x^{-\delta-1} - \frac{x^{-2\delta-1}}{R^2}\right) e^{-p\lambda_0\pi\left(2x^{-\delta} - \frac{x^{-2\delta}}{R^2}\right)}, \tag{2.26}$$

where $\delta \triangleq 2/\alpha$. With deterministic channels, a simple lower bound on the outage probability is derived using the nearest-interferer approximation:

$$\begin{aligned} p_{\mathrm{o}}^{\mathrm{nf}}(\theta) \triangleq \mathbb{P}\left(\frac{1}{I} < \theta\right) &\geqslant \mathbb{P}\left(\frac{1}{I_1} < \theta\right) \\ &= 1 - F_{I_1}(\theta^{-1}) \triangleq \underline{p}^{\mathrm{nf}}(\theta). \end{aligned}$$

Calculating explicitly, we have

$$\underline{p}^{\mathrm{nf}}(\theta) = 1 - \exp\left(-p\lambda_0\pi\left(2\theta^{\delta} - \frac{\theta^{2\delta}}{R^2}\right)\right). \tag{2.27}$$

2.4.2.2 Interference in finite networks with fading

When channels are subject to multi-path fading, the interference power from the nearest interferer is $h_1 I_1$, where h_1 is the multi-path fading coefficient. Then a lower bound of the outage probability is given by

$$\underline{p}^{\mathrm{f}}(\theta) = \mathbb{E}_H\left[\mathbb{P}\Big(I_1 > \frac{H}{\theta} \mid H\Big)\right],$$

where $H \triangleq h/h_1$ and h is the fading gain in the desired link. In the Rayleigh fading case, the pdf of H is given by

$$f_H(x) = \frac{1}{(x+1)^2}.$$

We then obtain

$$\underline{p}^{\mathrm{f}}(\theta) = 1 - \int_0^{\infty} \frac{\exp\left(-p\lambda_0\pi\left(2\theta^{\delta}x^{-\delta} - \frac{\theta^{2\delta}x^{-2\delta}}{R^2}\right)\right)}{(x+1)^2}\mathrm{d}x. \tag{2.28}$$

The lower bounds of the outage probabilities and the simulation results are presented in Fig. 2.4. For comparison, the lower bounds and simulation results under the RW

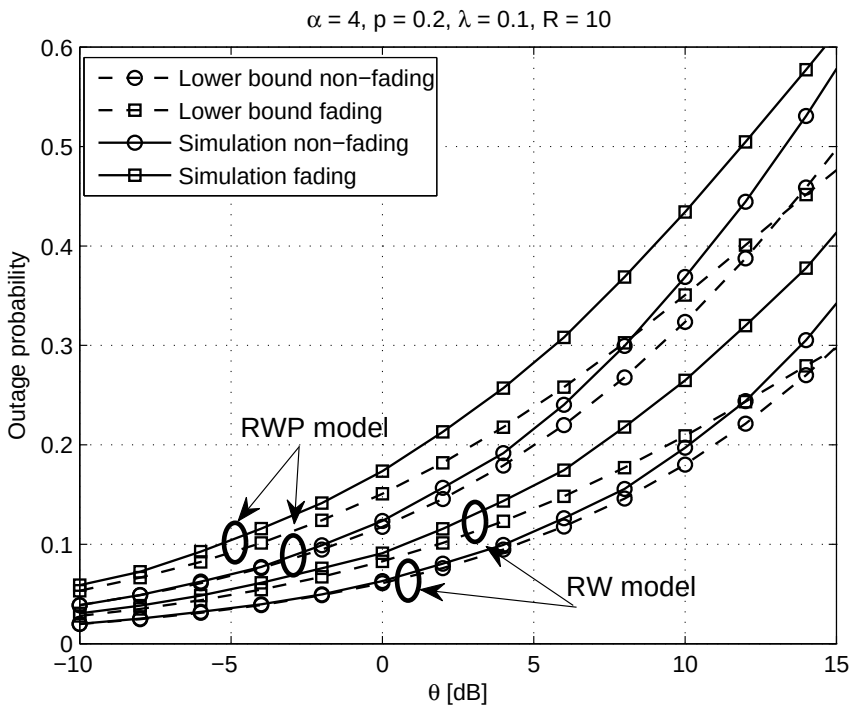

Figure 2.4. Simulation results versus the corresponding lower bounds of the outage probability for different fading and mobility models.

model are also included. The expected number of nodes in the region $\mathbb{E}[M] = 10\pi \approx 31$. From the figure, we find that the nearest-interferer approximation provides a close approximation in terms of the outage probability, in particular in the lower threshold regime (small θ), which is the regime of practical interest. Furthermore, multi-path fading is harmful to the link connections in mobile networks.

2.4.2.3 Interference in infinite networks

In infinite networks ($\mathbb{D} = \mathbb{R}^2$), the RWP model cannot be properly defined. However, we can derive the Laplace transform of the total interference if the node distance distribution follows (2.8). The Laplace transform of the interference is first calculated under a finite radius R, and then we let $R \to \infty$. Since the mobility model itself can not be defined, such a result is not the interference characterization under

the RWP model in infinite networks, but it provides an asymptotic expression as R gets large.

Proposition 2.5. *For $R \to \infty$, the Laplace transform of the total interference under RWP converges to*

$$\mathcal{L}_I(s) = \exp\Big(-2\pi\lambda_0 p s^{\delta}\mathbb{E}[h^{\delta}]\Gamma\left(1-\delta\right)\Big). \tag{2.29}$$

Proof. We start with a finite network of radius R. From (2.9), the radial transmitter intensity function is given by

$$\lambda(r) = 4p\lambda_0\pi r - \frac{4p\lambda_0\pi r^3}{R^2}.$$

Using the probability generating functional (pgfl) to calculate the Laplace transform, we obtain

$$\mathcal{L}_I(s) = \exp\left(-\mathbb{E}_h\Big[\underbrace{\int_0^R\Big(1-\exp\Big(-shr^{-\alpha}\Big)\Big)\lambda(r)\mathrm{d}r}_{A(h)}\Big]\right). \tag{2.30}$$

For the integral $A(h)$, we have

$$\begin{aligned} A(h) = &\int_0^R 4\pi p\lambda_0 r\Big(1-e^{-shr^{-\alpha}}\Big)\mathrm{d}r - \frac{p\lambda_0\pi}{R^{-2}}\Big(1-e^{-shR^{-\alpha}}\Big) \\ &- \int_0^R \frac{\alpha p\lambda_0\pi shr^{-\alpha+3}}{R^2}e^{-shr^{-\alpha}}\mathrm{d}r. \end{aligned}$$

Letting $R \to \infty$ and using the L'Hopital's rule, we obtain

$$\lim_{R\to\infty}\frac{1-e^{-shR^{-\alpha}}}{R^{-2}} = \frac{\alpha shR^{-\alpha-1}e^{-shR^{-\alpha}}}{-2R^{-3}} \overset{(a)}{=} 0,$$

where (a) holds for $\alpha > 2$, and

$$\lim_{R\to\infty} \int_0^R \frac{r^{-\alpha+3}}{R^2} e^{-shr^{-\alpha}} \mathrm{d}r = \lim_{R\to\infty} \frac{R^{-\alpha+2} e^{-shR^{-\alpha}}}{2} = 0.$$

Therefore, we have

$$\lim_{R\to\infty} A(h) = 2\lambda_0 \pi s^\delta h^\delta \Gamma(1-\delta).$$

Inserting this into (2.30) yields the result. □

Comparing (2.29) with [17, (18)], we notice that at the center of a large disk, the interference generated by RWP nodes is asymptotically equivalent to the interference generated by nodes of uniformly mobility with *doubled* node intensity as the disk radius $R \to \infty$, which is in agreement with (2.15). Without fading, the outage probability ($\alpha = 4$) is given by

$$p_{\mathrm{o}}^{\mathrm{nf}}(\theta) = \mathbb{P}(I > \theta^{-1}) = \mathrm{erf}\left(p\pi^{\frac{3}{2}}\sqrt{\theta}\lambda_0\right), \tag{2.31}$$

where $\mathrm{erf}(x) = 2\int_0^x e^{-t^2}\mathrm{d}t/\sqrt{\pi}$ is the error function.

Fig. 2.5 shows the outage probabilities for RWP nodes with different radii R by simulations versus the asymptotic bound. The bound, which is exact for $R \to \infty$, is calculated using (2.31). The simulation curves approach the bound quickly as R increases. Hence, (2.31) can be viewed as the upper bound and the asymptotic expression of the outage probability for large R. For Rayleigh fading, since $\mathbb{E}[h^\delta] = \Gamma(1+\delta)$,

$$p_{\mathrm{o}}^{\mathrm{f}}(\theta) = 1 - \mathcal{L}_I(\theta) = 1 - \exp\left(-\frac{2p\pi^2\lambda_0\delta\theta^\delta}{\sin(\pi\delta)}\right). \tag{2.32}$$

The same extra factor 2 is obtained as we compare (2.32) to the homogeneous case [34, (6)], which confirms that RWP mobility increases the interference and outage at the origin.

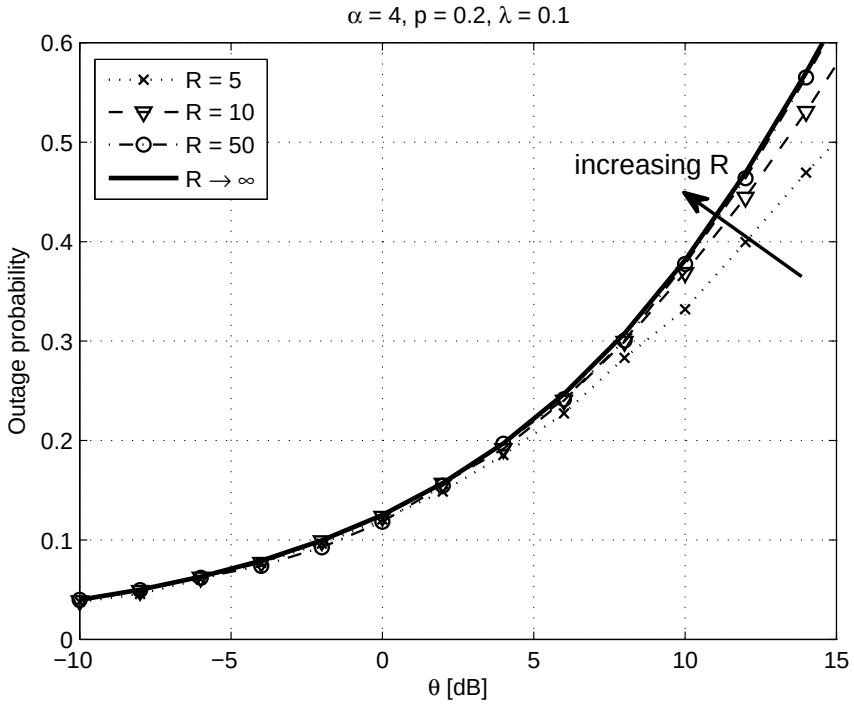

Figure 2.5. The outage probabilities under the RWP mobility with different radii R for the case without fading. The bound (solid curve) is obtained from (2.31). The curves with finite R are simulation results.

2.4.3 Tightness of the outage lower bound

In this part, we evaluate the tightness of the outage lower bound we have obtained in finite networks. For deterministic or Rayleigh fading channel, we have the following proposition.

Proposition 2.6. *When $\theta \to 0$, the outage probability $p_{\mathrm{o}}(\theta)$ and the outage lower bound $\underline{p}(\theta)$ have the following relationship*

$$\underline{p}(\theta) \sim p_{\mathrm{o}}(\theta). \tag{2.33}$$

Proof. First we consider the case without multi-path fading. With similar steps in [17], the ccdf of the interference in the infinite case is given by

$$F_I(x) = \frac{1}{\pi} \sum_{k=1}^{\infty} \frac{\Gamma(\alpha k)}{k!} \left(\frac{2\lambda_0 p \pi \Gamma(1-\delta)}{x^{\delta}} \right)^k \sin(k\pi(1-\alpha)). \tag{2.34}$$

The term $2\lambda_0$ in (2.34) instead of λ_0 in [17, (23)] is the difference between the RWP and uniform mobility cases. We then have

$$\begin{aligned}
\lim_{\theta \to 0} \frac{\underline{p}^{\mathrm{nf}}(\theta)}{p_{\mathrm{o}}^{\mathrm{nf}}(\theta)} &= \lim_{\theta \to 0} \frac{1 - \exp\left(-p\lambda_0 \pi \left(2\theta^{\delta} - \frac{\theta^{2\delta}}{R^2}\right)\right)}{\frac{1}{\pi} \sum_{k=1}^{\infty} \frac{\Gamma(\alpha k)}{k!} \left(2\lambda_0 p \pi \Gamma(1-\delta)\theta^{\delta}\right)^k} \\
&\overset{(a)}{=} \lim_{\theta \to 0} \frac{p\lambda_0 \pi^2 \left(2\delta\theta^{\delta-1} - \frac{2\delta\theta^{2\delta-1}}{R^2}\right) e^{-p\lambda_0 \pi \left(2\theta^{\delta} - \frac{\theta^{2\delta}}{R^2}\right)}}{\sum_{k=1}^{\infty} \frac{\Gamma(\alpha k)}{k!} \delta k \theta^{\delta k - 1} \left(2\lambda_0 p \pi \Gamma(1-\delta)\right)^k} \\
&\overset{(b)}{=} 1,
\end{aligned}$$

where (a) holds because of the L'Hopital's rule; (b) holds because of the dominance of the term for $k = 1$ in the Taylor series expansion.

Second, we consider Rayleigh fading. From (2.28) and (2.32), we have

$$\begin{aligned}
&\lim_{\theta\to 0}\frac{p^{\mathrm{f}}(\theta)}{p^{\mathrm{f}}_{\mathrm{o}}(\theta)} \\
&\quad\overset{(a)}{=}\lim_{\theta\to 0}\frac{\int_0^\infty \frac{x^{-\delta}}{(x+1)^2}\exp\left(-p\lambda_0\pi\left(2\theta^\delta x^{-\delta}-\frac{\theta^{2\delta}x^{-2\delta}}{R^2}\right)\right)\mathrm{d}y}{\frac{\pi\delta}{\sin(\pi\delta)}\exp\left(-\frac{2p\pi^2\lambda_0\delta\theta^\delta}{\sin(\pi\delta)}\right)} \\
&\quad= 1, \qquad (2.35)
\end{aligned}$$

where (a) holds because of L'Hopital's rule. □

2.5 Summary

In this section, we summarize the results we have obtained in this chapter and draw conclusions.

- *Macroscopic mobility:* We treat macroscopic mobility from a large-scale fading perspective. Fluctuations of the path loss induced by mobility constitute another type of fading in wireless channels besides multi-path effects. To make the difference clear, we may speak of fading induced by microscopic mobility (multi-path fading) and fading induced by macroscopic mobility.

- *Mean interference:* The mean interference at the center under the RWP model is asymptotically twice the interference under UMM, while the interference at the border is lower. Also for RWP, the interference at the border decreases to zero as the network radius goes large. These observations lead us to an important research direction: the design of location-aware routing algorithms. However, the decreasing interference is due to the smaller node intensity near the border, which means that fewer nodes can be chosen as receivers. The trade-off between the locations of destinations (or relays) and the interference should be considered.

- *Interference distribution and outage probability:* The uniform mobility models do not affect the interference distribution compared to the static network. However, the RWP nodes generate more interference at the origin, which leads to higher outage probability. The nearest-interferer approximation provides a tight lower bound on the outage probability especially in low threshold regime.

CHAPTER 3

INTERFERENCE AND OUTAGE IN MOBILE RANDOM NETWORKS: TEMPORAL CORRELATION

3.1 Introduction

The interference statistics in mobile networks in a single time slot have been studied in the previous chapter, with concrete results also for the outage statistics. However, only investigating the interference in a single time slot is insufficient to design the transmission and routing schemes in wireless networks, since the interference is temporally and spatially correlated. Such correlation, which is caused by the locations of mobile nodes, affects retransmission and routing strategies greatly. For example in an ARQ (Automatic Repeat reQuest) retransmission mechanism, a packet is retransmitted after a timeout or after a negative acknowledgment (NACK) received. Intuitively when a link is in outage and correlation is high, blind retransmissions lead to a higher failure rate than for independent interference. Quantifying such correlation is hence necessary. In this chapter, we consider uniform mobility models only and focus on infinite networks ($\mathbb{D} = \mathbb{R}^2$). We assume that $\epsilon > 0$ in the path-loss expression in (2.10), since for $\epsilon = 0$ some integrals (such as the mean interference) are infinite.

In [36], the spatio-temporal correlations of the interference and outage in static networks have been studied. The spatial distribution of link outages in static networks has been derived in [37]. To our knowledge, there is no prior work on the correlation of the interference in mobile networks. In this chapter, we mainly focus on mobile

Poisson networks. We quantify the temporal correlations of the interference and outage in terms of the correlation coefficient of the interference and conditional outage probability, respectively, under various mobility models.

The rest of the chapter is organized as follows. The temporal correlation of the interference in Poisson networks is presented in Section 3.2. Outage correlation is discussed in Section 3.3. Section 3.4 summarizes the chapter.

3.2 Temporal correlation of interference

In this section, we analyze the temporal correlation of the interference. The spatio-temporal correlation can be treated similarly. Because of the spatial stationarity of the point process, it is sufficient to consider the interference at the origin. The total interference in (2.11), $I(t)$, is identically distributed for any $t \in \mathbb{N}$. We denote the temporal correlation coefficient of the interference between time s and t as $\rho_\tau \triangleq \rho_{I(t)I(s)}$, where $\tau = |t-s|$. We have the following proposition about ρ_τ.

Proposition 3.1. *The temporal correlation coefficient of the interferences $I(s)$ and $I(t)$, where $s \neq t$, is given by*

$$\rho_\tau = \frac{p \int_{\mathbb{R}^2} g(x)\mathbb{E}_{w_\tau}[g(x+\bar{v}w_\tau)]\mathrm{d}x}{\mathbb{E}[h^2]\int_{\mathbb{R}^2} g^2(x)\mathrm{d}x} \leqslant \frac{p}{\mathbb{E}[h^2]}, \tag{3.1}$$

where $\bar{v}w_\tau$ is the location difference of a node between time s and t.

Proof. Since $I(s)$ and $I(t)$ are identically distributed, we have

$$\rho_\tau \triangleq \frac{\mathrm{Cov}(I(t), I(s))}{\mathrm{Var}[I(t)]} = \frac{\mathbb{E}[I(t)I(s)] - \mathbb{E}[I(t)]^2}{\mathbb{E}[I(t)^2] - \mathbb{E}[I(t)]^2}. \tag{3.2}$$

The mean product of $I(t)$ and $I(s)$ $(t \neq s)$ is given by

$$\begin{aligned}
&\mathbb{E}[I(t)I(s)] \\
&= \mathbb{E}\left[\sum_{x\in\Phi(t)} T_x(t)h_x(t)g(x)\sum_{y\in\Phi(s)} T_y(s)h_y(s)g(y)\right] \\
&= \mathbb{E}\left[\sum_{x\in\Phi(s)} T_x(t)h_x(t)g(x+\bar{v}w_\tau)\sum_{y\in\Phi(s)} T_y(s)h_y(s)g(y)\right] \\
&= \mathbb{E}\left[\sum_{x\in\Phi(s)} T_x(t)T_x(s)h_x(t)h_x(s)g(x+\bar{v}w_\tau)g(x)\right] + \\
&\quad \mathbb{E}\left[\sum_{x,y\in\Phi(s)}^{x\neq y} T_x(t)T_y(s)h_x(t)h_y(s)g(x+\bar{v}w_\tau)g(y)\right], \qquad (3.3)
\end{aligned}$$

where $\bar{v}w_\tau$ is the location difference of a node between time s and t. Conditioning on w_τ and following the proof of Lemma 1 in [36], we have the conditional temporal correlation coefficient $\rho(\tau \mid w_\tau)$ as

$$\rho(\tau \mid w_\tau) = \frac{p\int_{\mathbb{R}^2} g(x)g(x+\bar{v}w_\tau)\mathrm{d}x}{\mathbb{E}[h^2]\int_{\mathbb{R}^2} g^2(x)\mathrm{d}x}. \qquad (3.4)$$

Deconditioning on w_τ yields (3.1). Exploring $\mathbb{E}_{w_\tau}[g(x+\bar{v}w_\tau)]$ in (3.1), we obtain that ρ_τ decreases monotonically with $\bar{v}$. Hence ρ_τ is upper bounded by

$$\rho_\tau \leqslant \lim_{\bar{v}\to 0}\frac{p\int_{\mathbb{R}^2} g(x)\mathbb{E}_{w_\tau}[g(x+\bar{v}w_\tau)]\mathrm{d}x}{\mathbb{E}[h^2]\int_{\mathbb{R}^2} g^2(x)\mathrm{d}x} = \frac{p}{\mathbb{E}[h^2]}.$$

Proposition 3.1 is then proved. □

The spatio-temporal correlation coefficient of the interference at two given locations is provided in [36, (11)]. For mobile networks, the random position difference of the nodes in different time slots needs to be averaged out. The difference between the static and mobile networks is that in a static network, the path loss $g(x)$ does not change in one realization, while $g(x(t))$ is time variant in a mobile network. The

correlation coefficient is independent of the intensity λ_0, since the interference scales linearly with λ_0.

For a time difference τ, we express the pdf of w_τ as the sum of an atmoic and a diffuse part:

$$f_{w_\tau}(z) = \sum_{i=1}^{K} a_i \delta(z - z_i) + \tilde{f}(z), \tag{3.5}$$

where $\sum_i a_i \leqslant 1$ and a_i ($a_i > 0$) are the probability masses of w_τ at z_i; z_i are ordered according to the Euclidean distance to the origin ($0 \leqslant \|z_1\| \leqslant \|z_2\| \leqslant \cdots$); $\delta(\cdot)$ is an impulse function; $\tilde{f}(z)$ is right-continuous at z.

We also let $d_{\mathcal{H}} \triangleq \mathcal{H}(\mathrm{supp}(w_\tau))$, where $\mathcal{H}(\cdot)$ is the Hausdorff dimension and $\mathrm{supp}(x)$ is the support of the random variable x. We restrict ourselves to $d_{\mathcal{H}} \in \{0, 1, 2\}$. We now have the following theorem about the scaling property of ρ_τ.

Theorem 3.2. *If $K \geqslant 1$ and $z_1 = 0$, we have*

$$\rho_\tau \sim \frac{a_1 p}{\mathbb{E}[h^2]}, \qquad \bar{v} \to \infty, \tag{3.6}$$

where $a_1 = \mathbb{P}(w_\tau = 0)$. If $f_{w_\tau}(0) = 0$ and $K = 0$, we have

$$\rho_\tau \in o\left(\bar{v}^{-d_{\mathcal{H}}}\right). \tag{3.7}$$

If $f_{w_\tau}(0) > 0$, we have

$$\rho_\tau \in \Omega\left(\bar{v}^{-d_{\mathcal{H}}}\right). \tag{3.8}$$

For $K = 0$ and $f_{w_\tau}(0) > 0$, we have

$$\rho_\tau \in \Theta\left(\bar{v}^{-d_{\mathcal{H}}}\right). \tag{3.9}$$

For $d_{\mathcal{H}} = 2$ and $K = 0$, we have

$$\rho_\tau \bar{v}^2 \sim \frac{p f_{w_\tau}(0) \delta \epsilon^\delta \pi^2}{\mathbb{E}[h^2](1-\delta)\sin(\pi\delta)}. \tag{3.10}$$

Proof. Rewriting $\mathbb{E}_{w_\tau}[g(x + \bar{v} w_\tau)]$, we have

$$\begin{aligned}\mathbb{E}_{w_\tau}[g(x+\bar{v}w_\tau)] &= \sum_{i=1}^{K} a_i g(x+\bar{v}z_i) + \int_{\mathbb{R}^d} \frac{\tilde{f}(z)}{\epsilon + \|x+\bar{v}z\|^\alpha} \mathrm{d}z \\ &= \sum_{i=1}^{K} a_i g(x+\bar{v}z_i) + \frac{1}{\bar{v}^d} \int_{\mathbb{R}^d} \frac{\tilde{f}(t/\bar{v})}{\epsilon + \|x+t\|^\alpha} \mathrm{d}t\end{aligned} \tag{3.11}$$

Inserting this in (3.1) yields (3.6), (3.7), (3.8), and (3.9). For $d_{\mathcal{H}} = 2$ and $z_1 > 0$, we have

$$\lim_{\bar{v}\to\infty} \rho \bar{v}^2 = \frac{p f_{w_\tau}(0) \left(\int_{\mathbb{R}^2} g(x)\mathrm{d}x\right)^2}{\mathbb{E}[h^2]\mathbb{R}^2 g^2(x)\mathrm{d}x},$$

which yields (3.10), since

$$\int_{\mathbb{R}^2} g(x)\mathrm{d}x = \frac{\delta\pi^2}{\epsilon^{1-\delta}\sin(\pi\delta)},$$

and

$$\int_{\mathbb{R}^2} g^2(x)\mathrm{d}x = \frac{\delta(1-\delta)\pi^2}{\epsilon^{2-\delta}\sin(\pi\delta)}.$$

Theorem 3.2 is then proved. □

TABLE 3.1

THE SCALING PROPERTIES OF FOUR TYPES OF MOBILITY MODELS.

Models	$d_{\mathcal{H}}$	$f_{w_1}(z)$	Scaling property
The 1st model	2	$0.2\delta(z)+0.8\tilde{f}(z)$, where $\tilde{f}(z)=\begin{cases}\frac{1}{\pi R_1^2} & \|z\|\leqslant R_1\\ 0 & \text{otherwise,}\end{cases}$ where $R_1=15/8$	$\rho_1\sim\frac{0.2p}{\mathbb{E}[h^2]}$
The RW model	2	$\tilde{f}(z)=\begin{cases}\frac{1}{\pi R_{\mathrm{RW}}^2} & \|z\|\leqslant R_{\mathrm{RW}}\\ 0 & \text{otherwise}\end{cases}$	$\rho_1\bar{v}^2\sim\frac{p\delta\epsilon^{\delta}\pi}{\mathbb{E}[h^2](1-\delta)R_{\mathrm{RW}}^2\sin(\pi\delta)}$
The 3rd model	2	$\tilde{f}(z)=\begin{cases}\frac{4}{3\pi R_3^2} & R_3/2\leqslant\|z\|\leqslant R_3\\ 0 & \text{otherwise,}\end{cases}$ where $R_3=9/7$	$\rho_1\in o\left(\bar{v}^{-2}\right)$
The 4th model	1	$\tilde{f}(z)=\begin{cases}\frac{1}{4} & \|z\|\leqslant 2\\ 0 & \text{otherwise}\end{cases}$	$\rho_1\in\Theta\left(\bar{v}^{-1}\right)$

If a node stays in the same location in time s and t with positive probability, ρ_τ converges to a constant when $\bar{v}$ goes large, since the static portion asymptotically dominates the temporal correlation. On the other hand, if a node moves to other locations with probability 1, the decay of ρ_τ depends on the Hausdorff dimension $d_{\mathcal{H}}$ and $f_{w_\tau}(0)$. Given $\tau = 1$, Fig. 3.1 shows ρ_1 versus $\bar{v}$ under different artificial mobility models, which are described in Table 3.1.

Fig. 3.2 shows ρ_τ versus ϵ. When ϵ is small, ρ_τ increases with α. For α not too close to 2, interferers close to the origin dominate the interference. Such dominance is more prominent with larger α and hence causes higher temporal correlation of the interference. However, ρ_τ decreases with α when ϵ is large. More nodes contribute to the interference in this case. For large ϵ, the smaller the path loss exponent, the more correlated the interference is.

The integral $\int_{\mathbb{R}^2} g(x)\mathbb{E}_{w_\tau}[g(x+\bar{v}w_\tau)]\mathrm{d}x$ in (3.1) depends on the mobility models. In the next several subsections, we discuss different mobility models individually.

3.2.1 Constrained i.i.d. mobility (CIM)

Corollary 3.3. *The temporal correlation coefficient under the CIM model $\rho_{\tau,\mathrm{CIM}}$, where $\tau \geqslant 1$, is upper bounded by*

$$\rho_{\tau,\mathrm{CIM}} \lesssim \frac{p}{\mathbb{E}[h^2]} \cdot \min\left\{1, \frac{\delta\pi\epsilon^\delta}{(1-\delta)R_{\mathrm{CIM}}^2 \sin(\pi\delta)\bar{v}^2}\right\}, \tag{3.12}$$

where $R_{\mathrm{CIM}} = 45\pi/128$.

Proof. From (3.11) and the fact that $f_{w_\tau}(0) \geqslant f_{w_\tau}(x)$,

$$\mathbb{E}_{w_\tau}[g(x+\bar{v}w_\tau)] \leqslant \frac{1}{\bar{v}^2}\int_{\mathbb{R}^2} \frac{f_{w_\tau}(0)}{\epsilon + \|x+t\|^\alpha}\mathrm{d}t. \tag{3.13}$$

(3.12) follows from Theorem 3.2 after several steps of calculation, since $f_{w_\tau}(0) =$

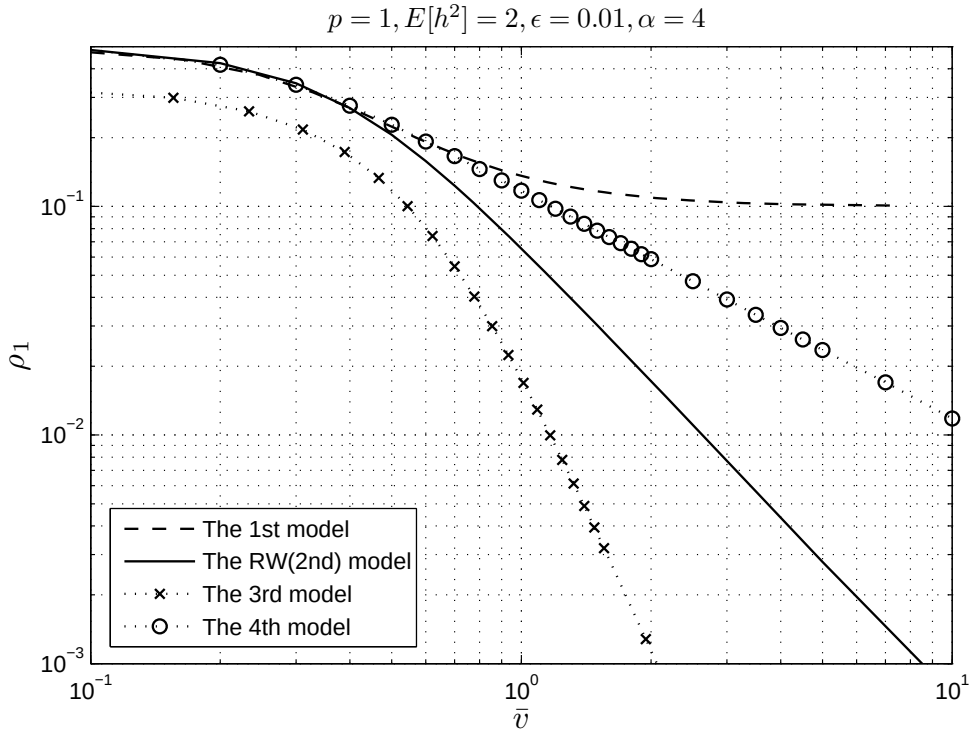

Figure 3.1. The temporal correlation coefficient ρ_1 versus the mean speed $\bar{v}$ under different mobility models.

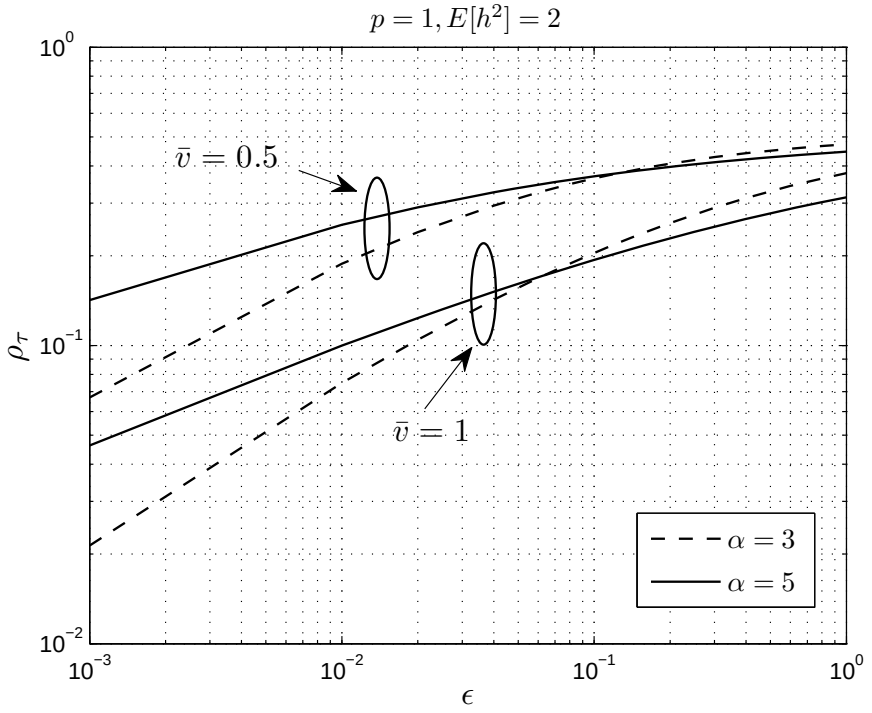

Figure 3.2. The temporal correlation coefficient ρ_τ versus ϵ under the CIM model.

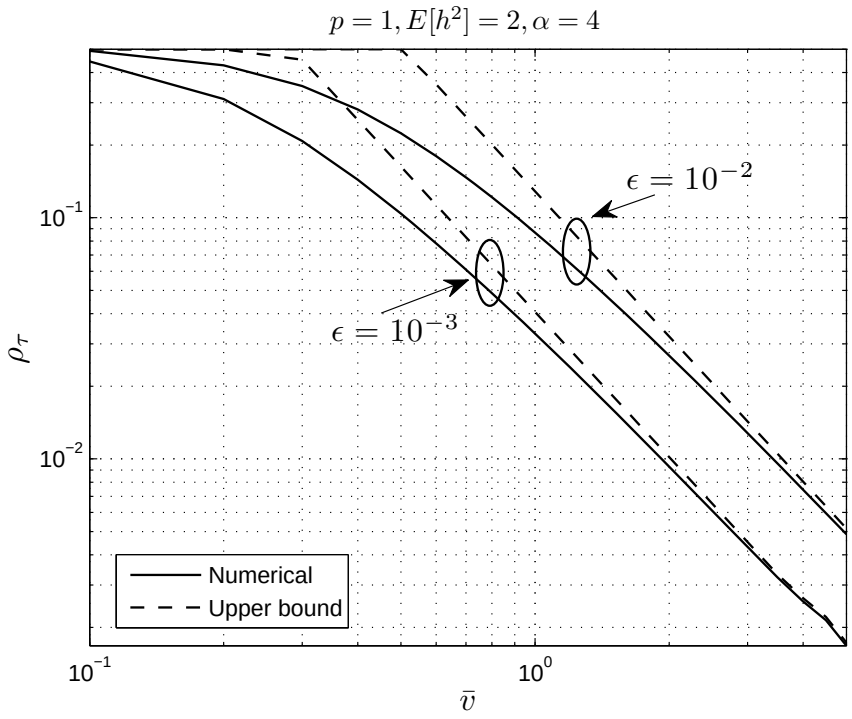

Figure 3.3. Numerical evaluation (from (3.1)) of the temporal correlation coefficient ρ_τ versus the mean node speed $\bar{v}$ with the corresponding upper bound (from (3.12)). The mobility model is CIM.

$1/\pi R_{\text{CIM}}^2$. □

Fig. 3.3 shows the numerical evaluation of $\rho_{\tau,\text{CIM}}$ from (3.1) (solid curves) together with the upper bound from (3.12) (dashed curves). The curves converge to the upper bound fast as $\bar{v}$ increases.

From (3.1) and (3.12), we find that the temporal correlation under the CIM model, $\rho_{\tau,\text{CIM}}$, is independent of τ. This observation is in agreement with the definition of the CIM model. For the Nakagami-m fading model, we have $\mathbb{E}[h^2] = \frac{m+1}{m}$. In particular, $\mathbb{E}[h^2] = 2$ for Rayleigh fading ($m = 1$), and $\mathbb{E}[h^2] = 1$ for no fading ($m \to \infty$). $\rho_{\tau,\text{CIM}}$ increases with m, as well as with the MAC scheme parameter p. Both fading and random MAC scheduling schemes reduce the temporal correlation of the interference.

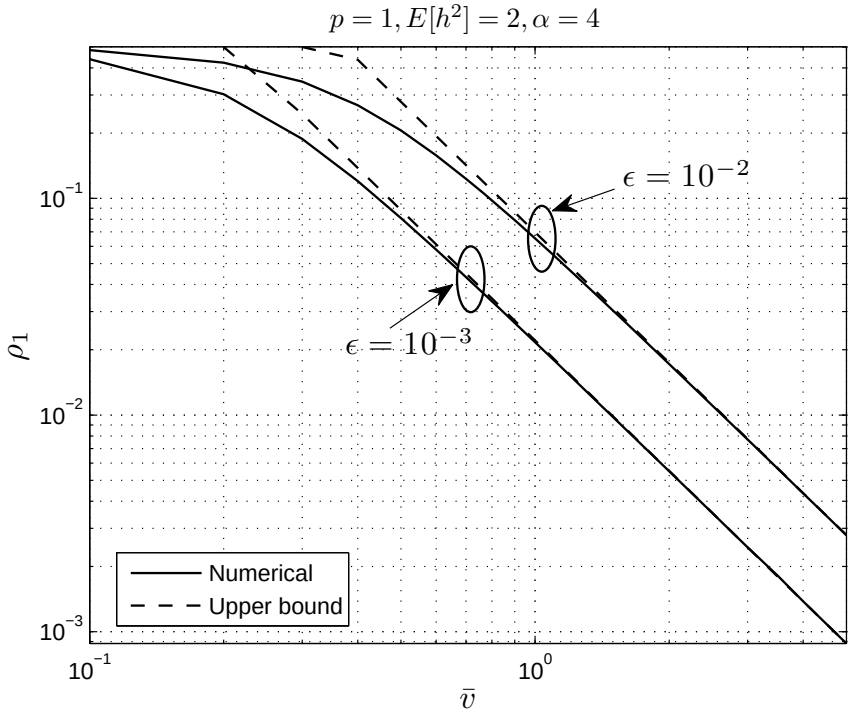

Figure 3.4. Numerical evaluation (from (3.1)) of the temporal correlation coefficient ρ_1 versus the mean node speed $\bar{v}$ with the corresponding upper bound (from (3.14)). The mobility model is RW.

3.2.2 Random walk (RW)

Under the RW model, we focus on the temporal correlation of the interference between two successive time slots, *i.e.*, ρ_1. By a similar derivation as for the CIM model, we have the following corollary about $\rho_{1,\mathrm{RW}}$.

Corollary 3.4. *The temporal correlation coefficient under the RW model $\rho_{1,\mathrm{RW}}$ is upper bounded by*

$$\rho_{1,\mathrm{RW}} \lesssim \frac{p}{\mathbb{E}[h^2]} \cdot \min\left\{1, \frac{4\delta\pi\epsilon^{\delta}}{9(1-\delta)\sin(\pi\delta)\bar{v}^2}\right\}. \tag{3.14}$$

Proof. The calculation is straightforward following the proof of Corollary 3.3 since $f_{w_1}(0) = 1/\pi R_{\mathrm{RW}}^2$. □

Fig. 3.4 displays the numerical evaluation of $\rho_{1,\mathrm{RW}}$ from (3.1) and its upper bound from (3.14). Again the convergence is fast.

3.2.3 Discrete-time Brownian motion (BM)

Under the BM model, we have

$$w_\tau = \sum_{i=1}^{\tau} w(i) \overset{(d)}{=} \sqrt{\tau} w_0,$$

where $\overset{(d)}{=}$ denotes the equality in distribution and w_0 is a two-dimensional Gaussian random variable, *i.e.*, $\mathcal{N}(0, \sigma_1^2\mathbf{I})$, where $\mathbf{I}$ is the 2-by-2 identity matrix. Hence, (3.1) can be rewritten as

$$\rho_{\tau,\mathrm{BM}} \;=\; \frac{p \int_{\mathbb{R}^2} g\,(x)\, \mathbb{E}_{w_0}[g(x + \sqrt{\tau}\bar{v}w_0)]\,\mathrm{d}x}{\mathbb{E}[h^2] \int_{\mathbb{R}} g^2(x)\mathrm{d}x}. \tag{3.15}$$

Fig. 3.5 plots ρ_1 versus the mean speed of nodes $\bar{v}$ under three mobility models. As we observe from the figure, ρ_1 under these three models are asymptotically proportional

to $\bar{v}^{-2}$. At an identical speed level, ρ_1 under these three models are close. For large τ, we have the following corollary about $\rho_{\tau,\mathrm{BM}}$.

Corollary 3.5. *When the time difference $\tau \to \infty$, the temporal correlation coefficient under the BM model is given by*

$$\rho_{\tau,\mathrm{BM}} \sim C\tau^{-1}, \tag{3.16}$$

where

$$C = \frac{\pi^2 \epsilon^\delta}{\delta(1-\delta)\sin(\pi\delta)\bar{v}^2},$$

and $\rho_{\tau,\mathrm{BM}}$ is upper bounded by

$$\rho_{\tau,\mathrm{BM}} \lesssim \frac{p}{\mathbb{E}[h^2]} \cdot \min\left\{1, \frac{\pi^2 \epsilon^\delta}{\delta(1-\delta)\sin(\pi\delta)\tau\bar{v}^2}\right\}. \tag{3.17}$$

Proof. Based on Theorem 3.2, (3.16) and (3.17) follow from (3.15) after a few elementary steps. □

3.3 Outage correlation

In the design of retransmission schemes in wireless networks, it is often assumed that outage events are independent across time for the sake of mathematical simplicity. However, due to the temporal correlation of the interference, link outage events are temporally correlated as well. Intuitively speaking, a link in outage at a given time indicates a higher outage probability in the next several time slots. Such correlation affects retransmission and routing schemes greatly and thus needs to be quantified. The correlation of link outage in static networks is examined in [36]. In this section, we discuss the temporal correlation of the outage in mobile networks. Rayleigh fading is assumed in the analysis.

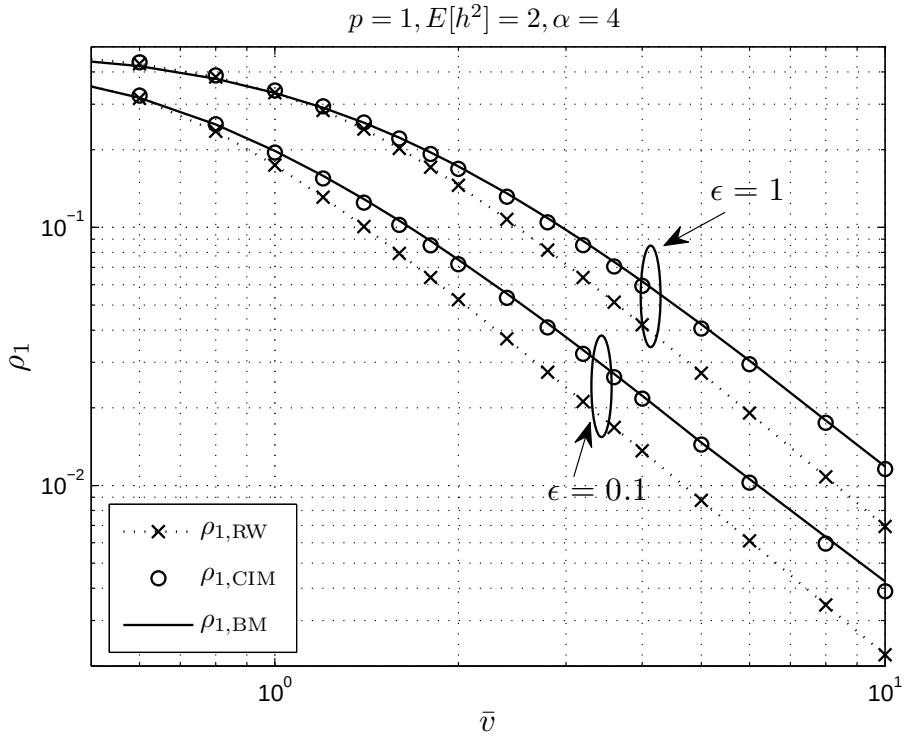

Figure 3.5. The interference correlation coefficient ρ_1 versus the mean speed $\bar{v}$ under three mobility models.

$$
\begin{aligned}
\mathbb{P}(A_s, A_t) &= \mathbb{P}(h(s) < \theta I(s), h(t) < \theta I(t)) \\
&\overset{(a)}{=} \mathbb{E}_{I(s),I(t)}\left[(1-\exp\left(-\theta I(s)\right))(1-\exp\left(-\theta I(t)\right))\right], \\
&\overset{(b)}{=} 1 - 2\mathbb{E}[\exp(-\theta I(t))] + \\
&\quad \mathbb{E}\left[\exp\left(-\theta \sum_{x\in\Phi(s)} \left(T_x(s)h_x(s)g(x) + T_x(t)h_x(t)g(x+\bar{v}w_\tau)\right)\right)\right] \\
&\overset{(c)}{=} 1 - 2\mathcal{L}_I(\theta) + \\
&\quad \mathbb{E}\left[\prod_{x\in\Phi(s)} \left(\frac{p}{1+\theta g\left(x\right)} + 1 - p\right)\left(\frac{p}{1+\theta g\left(x+\bar{v}w_\tau\right)} + 1 - p\right)\right] \\
&\overset{(d)}{=} 1 - 2\mathcal{L}_I(\theta) + \mathbb{E}_{w_\tau}\left[\exp\left(-\lambda_0 \int_{\mathbb{R}^2} 1 - \left(\frac{p}{1+\theta g\left(x\right)} + 1 - p\right)\cdot\right.\right. \\
&\quad \left.\left.\left(\frac{p}{1+\theta g\left(x+\bar{v}w_\tau\right)} + 1 - p\right)\mathrm{d}x\right)\right]. \qquad (3.18)
\end{aligned}
$$

Let A_t denote the event that the link is in outage at time t, *i.e.*,

$$A_t \triangleq \left\{\mathrm{SIR}(t) = \frac{h(t)}{I(t)} < \theta\right\},$$

where the distance of the desired link is normalized to one as indicated in Section 2.2.1. The joint probability of the events A_s and A_t is given in (3.18), where (a) follows from the independence of $h(s)$ and $h(t)$; (b) follows from the identical distribution of $I(t)$ and $I(s)$; (c) follows from the averaging over T_x and h_x; (d) holds from the probability generating functional (pgfl) of the PPP.

The direct evaluation of (3.18) seems hopeless, since the joint distribution of the two correlated random variables $I(t)$ and $I(s)$ is hard to obtain. However, we find that $\mathbb{P}(A_s, A_t)$ is upper bounded by the joint outage probability in static networks.

Proposition 3.6. *The conditional outage probability* $\mathbb{P}(A_t \mid A_s)$ *is upper bounded by*

$$\mathbb{P}(A_t \mid A_s) \leqslant 1 - \mathcal{L}_I(\theta) + \frac{(B-1)\mathcal{L}_I^2(\theta)}{1-\mathcal{L}_I(\theta)}, \qquad (3.19)$$

where

$$B \triangleq \exp\left(\lambda_0 p^2 \int_{\mathbb{R}^2} \left(\frac{\theta g(x)}{1+\theta g(x)}\right)^2 \mathrm{d}x\right) = \exp\left(\frac{\delta\pi^2(1-\delta)\theta^2\lambda_0 p^2}{(\epsilon+\theta)^{2-\delta}\sin(\pi\delta)}\right). \tag{3.20}$$

Proof. We have

$$\mathbb{P}(A_t \mid A_s) = \frac{\mathbb{P}(A_t, A_s)}{\mathbb{P}(A_t)} \leqslant \lim_{\bar{v}\to 0} \frac{\mathbb{P}(A_t, A_s)}{\mathbb{P}(A_t)}.$$

The calculation of the joint outage probability in static networks ($\lim_{\bar{v}\to 0}\mathbb{P}(A_s, A_t)$) is similar to [36, Section IV] under the non-singular path-loss model. □

Corollary 3.7. *The conditional outage probability* $\mathbb{P}\left(A_t \mid \bar{A}_s\right)$ *is lower bounded by*

$$\mathbb{P}\left(A_t \mid \bar{A}_s\right) \geqslant 1 - B\mathcal{L}_I(\theta), \tag{3.21}$$

where B *is from (3.20).*

Proof. The proof is similar to the proof of Proposition 3.6. □

Fig. 3.6 and 3.7 display the simulation evaluations of the conditional outage probability versus the threshold θ and the MAC scheme parameter p, respectively, together with the upper and lower bounds from (3.19) and (3.21). The CIM model is used in the simulation. The unconditional outage probability $\mathbb{P}(A_t)$ is always smaller than $\mathbb{P}(A_t \mid A_s)$. The outage evaluation in a single time slot ignores the information about previous link states and thus provides an over-optimistic evaluation of the network performance. On the other hand, $\mathbb{P}(A_t) > \mathbb{P}\left(A_t \mid \bar{A}_s\right)$, as expected. The discrepancy between $\mathbb{P}(A_t \mid A_s)$ and $\mathbb{P}(A_t)$ is larger when $\mathbb{P}(A_t)$ is low (or θ is low), since the conditioning makes a larger difference in this regime. Conversely, the discrepancy between $\mathbb{P}\left(A_t \mid \bar{A}_s\right)$ and $\mathbb{P}(A_t)$ is larger when $\mathbb{P}(A_t)$ is high (θ is high).

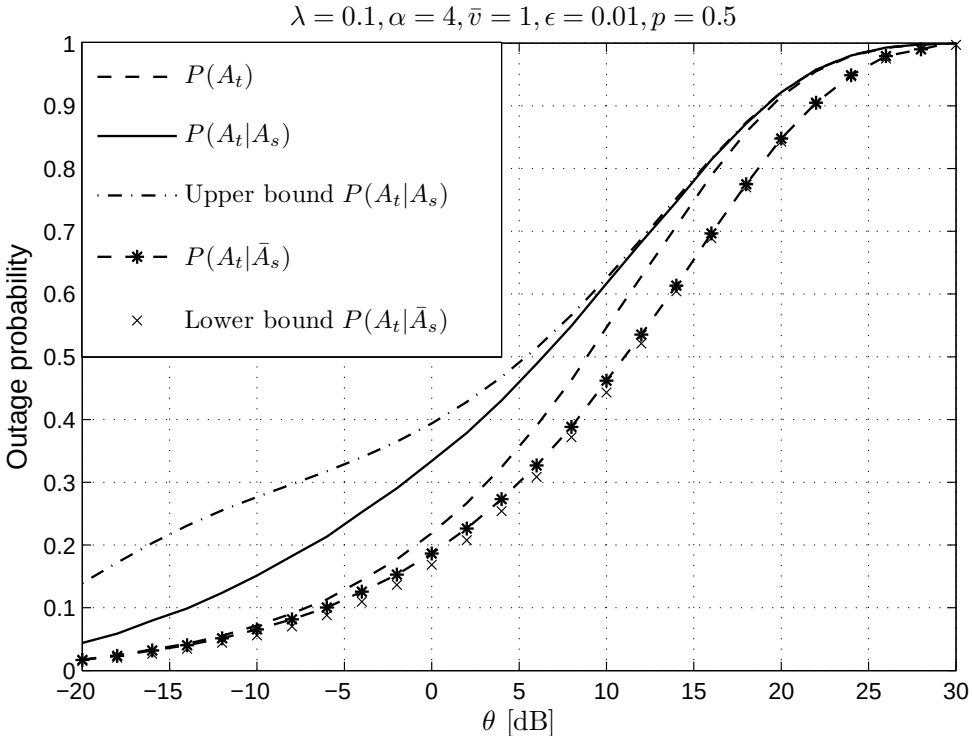

Figure 3.6. The conditional outage probabilities $\mathbb{P}(A_t \mid A_s)$ and $\mathbb{P}\Big(A_t \mid \bar{A}_s\Big)$ together with the unconditional outage probability $\mathbb{P}(A_t)$ versus the threshold θ under the CIM model. The dashed curve is the unconditional outage probability; the dash-dotted curve is the upper bound of $\mathbb{P}(A_t \mid A_s)$ from (3.19); the solid-line curve is the exact expression of $\mathbb{P}(A_t \mid A_s)$ via simulations; the stars are $\mathbb{P}(A_t \mid \bar{A}_s)$ via simulations; the $\times$ is the lower bound of $\mathbb{P}\Big(A_t \mid \bar{A}_s\Big)$ from (3.21).

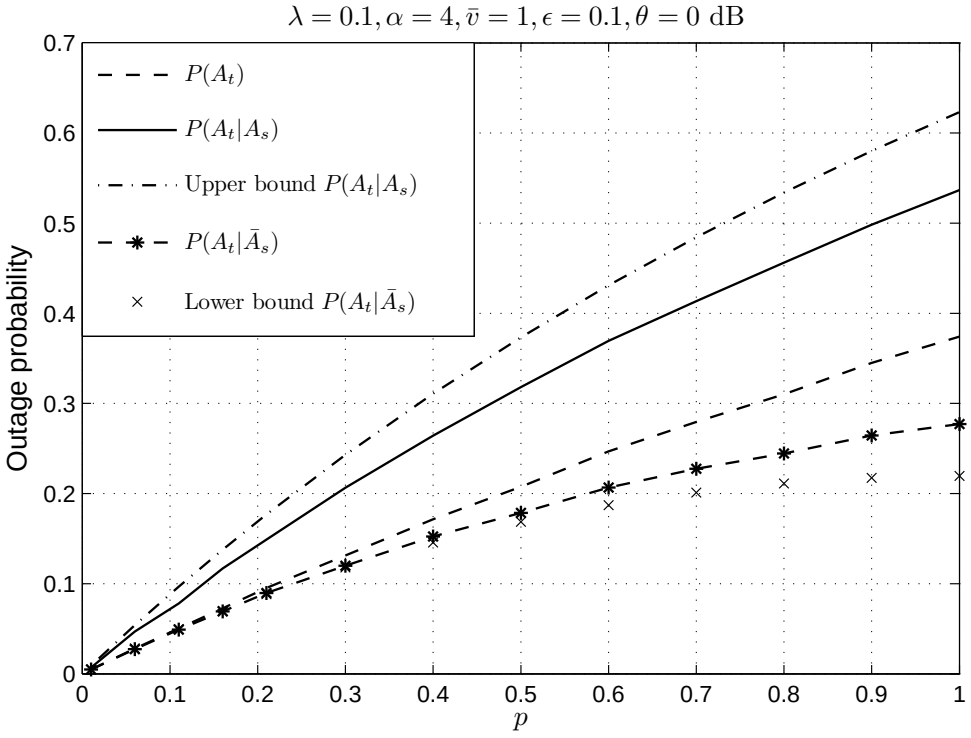

Figure 3.7. The conditional outage probabilities $\mathbb{P}(A_t \mid A_s)$ and $\mathbb{P}\big(A_t \mid \bar{A}_s\big)$ together with the unconditional outage probability $\mathbb{P}(A_t)$ versus the MAC scheme parameter p under the CIM model.

In the two extreme cases where the threshold $\theta \to \infty$ or $\theta \to 0$, the conditioning does not make a difference any more.

3.4 Summary

In this section, we summarize the results we have obtained in this chapter and draw conclusions.

- *Temporal correlation of interference:* The mobility models affect the correlation coefficient of the interference ρ. The more degrees of freedom the node explores, the faster ρ decays with the mobility range. Multi-path fading and random MAC schemes also reduce the interference correlation.

- *Temporal correlation of outage:* Conditioned on the link being in outage at time t, the outage probability in the next several time slots is higher compared to the unconditional outage probability. On the other hand, if a transmission is successful, the conditional success probability is higher in the next several time slots. Hence, the design of new retransmission schemes with correlation-awareness is important. For example, if a transmission is successful, the node should transmit more often in successive time slots (higher transmit probability) in order to take advantage of the outage (success) correlation. Conversely, if a link is in outage, several silence slots should be added before the transmitter starts another try, since blind retransmission worsens the network performance. If fewer transmitters are concurrent, the success probability increases due to the decreased interference power. It in turn lowers the number of retransmissions. The trade-off between delay and network throughput, and fairness and throughput should be explored as well.

CHAPTER 4

THE LOCAL DELAY IN MOBILE RANDOM NETWORKS

4.1 Introduction

In a wireless network, it is fundamentally necessary that every node is able to successfully transmit messages to at least one other node in the network in a finite amount of time. The local delay hence becomes an important quantity. Previous research in [14, 15] only focuses on two extreme cases, where the network is completely static or infintely mobile. In this chapter, we extend the local delay results under practical mobility models. Each node has a randomly chosen initial (home) location and a mobility region. Due to the temporal correlation of the node locations and interference, the events of successful transmission are temporally correlated, which strongly affects the local delay. Mobility helps reduce the temporal correlation of the interference and outage in large wireless networks [56]. Here, we evaluate its impact on the local delay.

The rest of the chapter is organized as follows. We introduce the system model in Section 4.2. The local delay for deterministic transmission distance is presented in Section 4.3. The local delay for random static transmission distance is discussed in Section 4.4. Section 4.5 presents the local delay for random time-variant transmission distance. Conclusions are drawn in Section 4.6.

4.2 System model

4.2.1 Transmitter process

Recall the system model introduced in Section 2.2. The potential transmitters in a network are randomly distributed on $\mathbb{R}^2$. Each of them has a home location and a mobility region. The home location process forms a PPP $\tilde{\Phi} = \{y_i\} \subset \mathbb{R}^2$ with intensity λ_0. $\tilde{\Phi}$ is assumed temporally static. Nodes make an excursion in the mobility region independently of each other at each time $t \in \mathbb{Z}$ with a certain probability. The definition of the mobility models will be given in Section 4.2.3. Hence at all times, the node location process forms another PPP $\Phi_t = \{x_i(t)\} \subset \mathbb{R}^2$ (correlated with $\tilde{\Phi}$) with the same intensity λ_0. If a transmitter is scheduled to transmit at time t, we assume that the transmission starts at the beginning of that time slot. Each transmission is finished within one time slot. Slotted ALOHA with parameter $p > 0$ is assumed as the MAC protocol.

4.2.2 Transmission scheme and receiver process

In Section 4.3 and 4.4, the receiver process does not affect the local delay calculation, since the transmission distance in the desired link is either deterministic or random static. In Section 4.5, we consider three transmission schemes: random bipolar, quasi-nearest-receiver, and nearest-receiver models. Different transmission schemes lead to different local delays in the network.

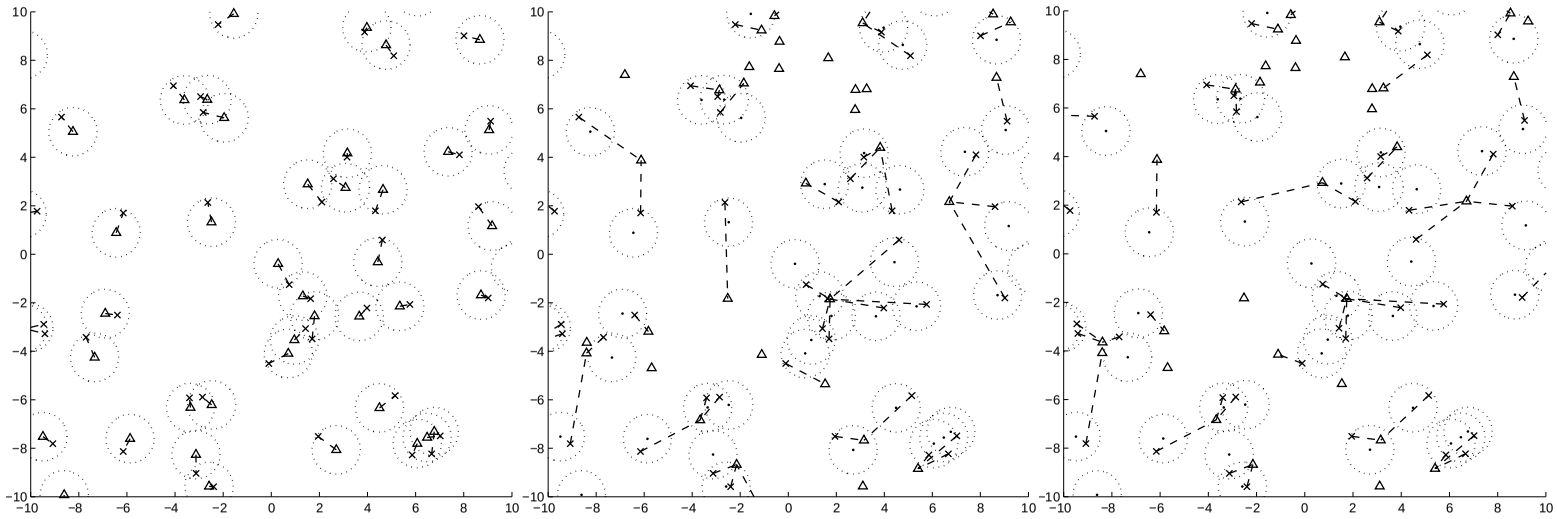

(a) Random bipolar model (b) Quasi-nearest-receiver model (c) Nearest-receiver model

Figure 4.1. Three types of transmission models. The triangles and crosses represent receivers and transmitters, respectively. The potential transmitter receiver pairs are connected by dashed lines. The transmitters are mobile in a circular region of radius $a_0 = 1$. The dotted circles represent their mobility regions. The network intensity $\lambda_0 = 0.1$. Under the random bipolar scheme (a), each transmitter has an assigned receiver, whose location is at the home location of the transmitter. Under quasi-nearest-receiver (b) and nearest-receiver (c) schemes, the receiver process, whose intensity is $\lambda' = 0.07$, is independent of the transmitter process. In (b), the assigned receiver is not always the nearest receiver to the transmitter, and the transmitter keeps transmitting to the same receiver. In (c), however, the transmitter always transmits to its nearest receiver.

4.2.2.1 Random bipolar model

We assume that each transmitter has an assigned receiver. The receivers are situated at the home locations of their assigned transmitters and stay fixed, *i.e.*, the receiver process is given by $\Psi = \tilde{\Phi}$. Those receivers can be thought of as randomly placed base stations. Each transmitter keeps transmitting to the same receiver. Figure 4.1(a) shows a realization of such a random bipolar network[1].

4.2.2.2 Quasi-nearest-receiver model

Here each transmitter conveys a message to a node that is close to the transmitter. We denote the receiver process as $\Psi = \{z_i\}$, which is a PPP with intensity λ' and independent of the transmitter process Φ_t. (Those nodes in Φ_t that are not scheduled to transmit are not available for reception.) Ψ is assumed temporally static. Each transmitter x_i chooses the receiver that is the closest to its home location $y_i \in \tilde{\Phi}$, *i.e.*,

$$z_i^* = \arg\min_{z \in \Psi} \{\|z - y_i\|\}.$$

We use the term "quasi-" to indicate that the receiver selected is not always the closest receiver to the transmitter's current position. A realization of the Poisson network with quasi-nearest-receiver transmission is shown in Figure 4.1(b).

4.2.2.3 Nearest-receiver model

Different from the quasi-nearest-receiver model, where the receiver is chosen based on the distance to a transmitter's home location, each transmitter $x_i(t)$ always picks

[1]The bipolar model usually has a fixed transmission distance (see Section 5.3 in [4]). In this model, however, the transmission distance is a random variable due to mobility.

the receiver that is the closest to it, *i.e.*,

$$z_i^*(t) = \arg\min_{z\in\Psi}\{\|z - x_i(t)\|\}$$

under the nearest-receiver model. A realization of the Poisson network with nearest-receiver transmission is shown in Figure 4.1(c).

The validity of quasi-nearest-receiver and nearest-receiver models depends on the frequency with which the nodes exchange their location information. If every node exchanges its location information with other nodes in each time slot t, we choose the nearest-receiver transmission scheme. If nodes do not (or seldom) exchange their location information, the quasi-nearest-receiver model is more appropriate. Hence, the difference between Figure 4.1(b) and 4.1(c) is that the transmitter keeps transmitting to the same receiver under the quasi-nearest-receiver scheme while it changes destinations in different time slots under the nearest-receiver scheme. Moreover, the transmission distance is not necessarily the shortest among all the potential receivers under the quasi-nearest-receiver scheme.

4.2.3 Mobility models

We use a constrained i.i.d. mobility (CIM) model, which was introduced in Section 2.2.2. Under CIM, the node locations in two different time slots are independent given the node's home location. We denote the pdf of the excursions by $f_w(x)$. Two specific models are considered.

Definition 4.1. *The node locations under the uniform mobility (UM) follow a uniform distribution in a ball of radius a_0 centered at the home location, i.e.,*

$$f_w(x) = \begin{cases} \frac{1}{\pi a_0^2} & \|x\| \leqslant a_0 \\ 0 & \text{otherwise,} \end{cases} \tag{4.1}$$

where $\|\cdot\|$ is the Euclidean distance.

The distance distribution between the home and the node locations is then given by

$$f_R(x) = \begin{cases} \frac{2x}{a_0^2} & x \leqslant a_0 \\ 0 & \text{otherwise.} \end{cases} \tag{4.2}$$

Definition 4.2. *The node locations under normal mobility model (NM) follow a symmetric normal distribution with variance σ^2 centered at the home location, whose pdf is given by*

$$f_w(x) = \frac{1}{2\pi\sigma^2} \exp\left(-\frac{\|x\|^2}{2\sigma^2}\right). \tag{4.3}$$

The distance distribution is given by the Rayleigh distribution

$$f_R(x) = \frac{x}{\sigma^2} \exp\left(-\frac{x^2}{2\sigma^2}\right). \tag{4.4}$$

We define $v_i(t) \triangleq \|x_i(t) - x_i(t-1)\|$. Let

$$\bar{v}_i(t) \triangleq \mathbb{E}\left[v_i(t)\right], \qquad \forall t \in \mathbb{Z}.$$

Due to ergodicity and point process homogeneity, the mean speed averaged over all nodes for a fixed time t is equal to the mean speed averaged over time for a fixed node. Hence, we drop i and t, and simply denote by $\bar{v}$ the mean speed of the node. For UM, we have $\bar{v} = 128a_0/45\pi$ [47, (8)] and for NM, we obtain $\bar{v} = \sqrt{\pi}\sigma$. The mean speed $\bar{v}$ is proportional to a_0 or σ. (a_0 is the identical to R_{CIM} in Chapter 3.)

The frequency at which nodes update their locations greatly affects the network geometry and performance. If nodes update their locations independently at time t with probability $1/K$, where $K > 1$, *i.e.*, $x_i(t) = y_i + w_i(t)$, where $w_i(t)$ is the random excursion, and stay at their previous locations with probability $1 - 1/K$, *i.e.*, $x_i(t) = x_i(t-1)$, we term this model *block mobility*. If the nodes update their

locations in each time slot t, we then have $x_i(t) = y_i + w_i(t)$ (or $K = 1$ in the *block mobility* case). In order to distinguish the cases where $K > 1$ and $K = 1$, we term $K = 1$ *fast mobility*. In the analysis, the interfering transmitters are always assumed mobile. The desired transmitter is assumed static in Section 4.3 and 4.4, and assumed mobile in Section 4.5.

4.2.4 Local delay definition

Let $\mathcal{S}$ be the static elements of a network. Assume the desired receiver[2] at the origin o, we let $\mathcal{C}_\mathcal{S}$ be the event that the receiver is successfully connected to its assigned transmitter in a single transmission conditioned on $\mathcal{S}$. The conditional success probability is given by

$$\mathbb{P}(\mathcal{C}_\mathcal{S}) = \mathbb{P}(\text{SIR} > \theta \mid \mathcal{S}),$$

where θ is a given threshold. If the receiver fails to decode a packet, it is retransmitted in the next scheduled transmission slot. Conditioned on $\mathcal{S}$, the success indicator random variables are temporally i.i.d. Hence, the distribution of the conditional local delay is geometric with mean $\mathbb{P}(\mathcal{C}_\mathcal{S})^{-1}$. The local delay is then the expectation with respect to (w.r.t.) $\mathcal{S}$:

$$D \triangleq \mathbb{E}_\mathcal{S}\left(\frac{1}{\mathbb{P}(\mathcal{C}_\mathcal{S})}\right). \tag{4.5}$$

D denotes the average number of slots that it takes the transmitter to successfully convey a packet to the receiver.

[2]In Section 4.3 and 4.4 the origin o does not belong to the receiver process Ψ. In Section 4.5, however, we need to slightly change the definition of the local delay.

4.3 Local delay for deterministic transmission distance

In this section, we present some basic results on the local delay, which will be used in the following sections. For completeness, the conditional Laplace transform of $I(t)$ given $\mathcal{S}$ in static networks ($\bar{v} = 0$) is given by

$$\mathcal{L}_0(s \mid \mathcal{S}) \triangleq \mathcal{L}_I(s \mid \mathcal{S} = \Phi) = \prod_{x \in \Phi} \left(1 - \frac{ps}{\|x\|^\alpha + s}\right), \tag{4.6}$$

whose derivation is presented in [15], and the unconditional Laplace transform of $I(t)$ in infinitely mobile networks ($\bar{v} = \infty$) is given by

$$\mathcal{L}_\infty(s) \triangleq \mathcal{L}_I(s \mid \mathcal{S} = \emptyset) = \exp\left(-\frac{\delta \lambda_0 p \pi^2 s^\delta}{\sin(\pi\delta)}\right), \tag{4.7}$$

where $\delta \triangleq 2/\alpha$.

We assume that the transmission distance is R. The interfering transmitters are mobile following the mobility models introduced in Section 4.2.3. Given R, we calculate the conditional local delay for the receiver at the origin. Two cases are considered: fast mobility and block mobility.

4.3.1 Fast mobility

If the excursions $w_i(t)$ are i.i.d. across time and space, the static elements of the network are $\mathcal{S} = \tilde{\Phi}$. We have the following proposition about the conditional Laplace transform of the interference and the conditional local delay.

Proposition 4.3. *Given the static elements of a network $\mathcal{S} = \tilde{\Phi}$, the conditional*

Laplace transform of the interference $\mathcal{L}_v(s \mid \mathcal{S})$ is given by[3]

$$\mathcal{L}_v(s\,|\,\mathcal{S}) \triangleq \mathcal{L}_I(s\,|\,\tilde{\Phi}) = \prod_{y\in\tilde{\Phi}} \left(1 - ps\int_{\mathbb{R}^2} \frac{f_w(x)}{\|y+x\|^{\alpha}+s}\mathrm{d}x\right), \tag{4.8}$$

where $f_w(x)$ is the pdf of the excursion vector. Given a transmission distance R, the conditional local delay is given by

$$D_v(\theta \mid R) = \frac{1}{p}\exp\left(\lambda_0 \int_{\mathbb{R}^2}\left(\frac{1}{1-p\theta R^{\alpha}\int_{\mathbb{R}^2}\frac{f_w(x)}{\|y+x\|^{\alpha}+\theta R^{\alpha}}\mathrm{d}x} - 1\right)\mathrm{d}y\right). \tag{4.9}$$

Proof. From (2.11), the total interference at the origin is given by

$$I(t) = \sum_{x\in\Phi_t} T_x(t)h_x(t)\,\|x\|^{-\alpha} = \sum_{y\in\tilde{\Phi}} T_y(t)h_y(t)\,\|y+w\|^{-\alpha}.$$

The conditional Laplace transform of the interference given $\tilde{\Phi}$ is thus given by

$$\begin{aligned}
\mathcal{L}_I(s \mid \tilde{\Phi}) &= \mathbb{E}\left[e^{-sI(t)} \mid \tilde{\Phi}\right] \\
&\overset{(a)}{=} \mathbb{E}\left[\exp\left(-s\sum_{y\in\tilde{\Phi}} T_y h_y\,\|y+w\|^{-\alpha}\right)\middle|\,\tilde{\Phi}\right] \\
&\overset{(b)}{=} \exp\left(\sum_{y\in\tilde{\Phi}}\log\left(1 - ps\int_{\mathbb{R}^2}\frac{f_w(x)}{\|y+x\|^{\alpha}+s}\mathrm{d}x\right)\right) \\
&= \prod_{y\in\tilde{\Phi}}\left(1 - ps\int_{\mathbb{R}^2}\frac{f_w(x)}{\|y+x\|^{\alpha}+s}\mathrm{d}x\right),
\end{aligned}$$

where (a) holds since the interferences $I(t)$ are exchangeable; (b) follows from [3,

[3]Similar to $\mathcal{L}_0(s \mid \mathcal{S})$ and $\mathcal{L}_\infty(s)$, the subscript v in $\mathcal{L}_v(s \mid \mathcal{S})$ indicates a mobile network, where the nodes are with finite mean speed.

Lemma 16.6.5] and averaging over the random excursions. Furthermore, we have

$$D_v(\theta \mid R) \triangleq \mathbb{E}_{\tilde{\Phi}}\left(\frac{1}{p\mathcal{L}_I(s \mid \tilde{\Phi})}\right)\Bigg|_{s=\theta R^{\alpha}},$$

where the term $p\mathcal{L}_I(s \mid \tilde{\Phi})$ is the probability that the scheduled transmitter successfully transmits a packet. (4.9) is then imminent from (4.8) using the probability generating functional (pgfl) of the PPP. □

The following corollary is then straightforward.

Corollary 4.4. *Given a transmission distance R, the local delay is lower bounded by*

$$D_v(\theta \mid R) \geqslant D_{\infty}(\theta \mid R).$$

Proof. From the definition of the local delay, we have

$$D_v(\theta \mid R) \overset{(a)}{\geqslant} \frac{1}{p\mathbb{E}_{\tilde{\Phi}}\left(\mathcal{L}_I(\theta \mid \tilde{\Phi})\right)} = \frac{1}{p\mathcal{L}_{\infty}(\theta)} = D_{\infty}(\theta \mid R), \tag{4.10}$$

where (a) holds due to Jensen's inequality. □

The following proposition provides an upper bound of $D_v(\theta \mid R)$.

Proposition 4.5. *Let $a = a_0$ under UM and $a = \sqrt{2}\sigma$ under NM. The conditional local delay given a transmission distance R is upper bounded by*

$$D_v(\theta \mid R) \leqslant \begin{cases} \frac{1}{p}\exp\left(\frac{\lambda_0 \pi p \gamma a^2 R^2}{\pi a^2 - p\gamma R^2}\right) & a\beta > R \\ D_0(\theta \mid R) & \text{otherwise,} \end{cases} \tag{4.11}$$

where

$$D_0(\theta \mid R) = \frac{1}{p}\exp\left(\frac{\lambda_0 p \gamma R^2}{q^{1-\delta}}\right), \tag{4.12}$$

$q = 1 - p$, *and*

$$\gamma \triangleq \frac{\delta \pi^2 \theta^\delta}{\sin(\pi\delta)} \tag{4.13}$$

is the spatial contention (see [15, (4)]*), and* $\beta \triangleq \sqrt{(1 - q^{1-\delta})\,\pi / p\gamma}$.

Proof. We first prove a general (looser) upper bound that $D_v(\theta \mid R) \leqslant D_0(\theta \mid R)$. Since

$$\int_{\mathbb{R}^2} \frac{f_w(x)}{\|y + x\|^\alpha + \theta R^\alpha} \mathrm{d}x \leqslant \frac{1}{\|y\|^\alpha + \theta R^\alpha},$$

we have

$$\begin{aligned} D_v(\theta \mid R) &\leqslant \lim_{a \to 0} \mathbb{E}_{\tilde{\Phi}} \left(\frac{1}{p \mathcal{L}_I(\theta \mid \tilde{\Phi})} \right) \\ &= \frac{1}{p} \exp\left(\frac{\delta \pi^2 p \lambda_0 \theta^\delta R^2}{q^{1-\delta} \sin(\pi\delta)} \right) = D_0(\theta \mid R). \end{aligned}$$

Next we prove a tighter upper bound for large a ($a = a_0$ under UM, and $a = \sqrt{2}\sigma$ under NM). We first consider UM. From (4.1) and (4.9), we have

$$\begin{aligned} &D_v(\theta \mid R) \\ &= \frac{1}{p} \exp\left(\lambda_0 \int_{\mathbb{R}^2} \left(\frac{1}{1 - p\theta R^\alpha \int_{\mathbb{R}^2} \frac{f_w(z-y)}{\|z\|^\alpha + \theta R^\alpha} \mathrm{d}z} - 1 \right) \mathrm{d}y \right) \\ &= \frac{1}{p} \exp\left(\lambda_0 \int_{B(0,a_0)} \left(\frac{1}{1 - \frac{p\theta R^\alpha}{\pi a_0^2} \int_{B(y,a_0)} \frac{1}{\|z\|^\alpha + \theta R^\alpha} \mathrm{d}z} - 1 \right) \mathrm{d}y \right) \cdot \\ &\quad \exp\left(\lambda_0 \int_{\mathbb{R}^2 \setminus B(0,a_0)} \left(\frac{1}{1 - \frac{p\theta R^\alpha}{\pi a_0^2} \int_{B(y,a_0)} \frac{1}{\|z\|^\alpha + \theta R^\alpha} \mathrm{d}z} - 1 \right) \mathrm{d}y \right) \qquad (4.14) \\ &\overset{(a)}{\leqslant} \frac{1}{p} \exp\left(\lambda_0 \int_{B(0,a_0)} \left(\frac{1}{1 - \frac{p\theta R^\alpha}{\pi a_0^2} \int_{\mathbb{R}^2} \frac{1}{\|z\|^\alpha + \theta R^\alpha} \mathrm{d}z} - 1 \right) \mathrm{d}y \right), \\ &\qquad\qquad a_0 > R\sqrt{\frac{p\gamma}{\pi}} \qquad (4.15) \\ &= \frac{1}{p} \exp\left(\frac{\lambda_0 \pi a_0^2 p \gamma R^2}{\pi a_0^2 - p\gamma R^2} \right), \qquad a_0 > R\sqrt{\frac{p\gamma}{\pi}}, \qquad (4.16) \end{aligned}$$

where (a) holds when $a_0 > R\sqrt{p\gamma/\pi}$ due to the fact that $o \notin \lim_{a_0\to\infty} B(ca_0, a_0)$ for any $c > 1$; the second exponential component in (4.14) hence goes to 0 for large a_0. On the other hand, we have another upper bound $D_v(\theta \mid R) \leqslant D_0(\theta \mid R)$. Taking the minimum of (4.16) and $D_0(\theta \mid R)$ yields (4.11), since $\pi a^2(1-q^{1-\delta}) > p\gamma R^2$ implies that $\pi a^2 > p\gamma R^2$.

For NM, we have

$$\begin{aligned}
&D_v(\theta \mid R)\\
&=\frac{1}{p}\exp\left(\lambda_0\int_{\mathbb{R}^2}\left(\frac{1}{1-\frac{p\theta R^\alpha}{2\pi\sigma^2}\int_{\mathbb{R}^2}\frac{\exp\left(-\|z-y\|^2/2\sigma^2\right)}{\|z\|^\alpha+\theta R^\alpha}\mathrm{d}z}-1\right)\mathrm{d}y\right)\\
&\overset{(a)}{\leqslant}\frac{1}{p}\exp\left(\lambda_0\int_{\mathbb{R}^2}\left(\frac{1}{1-\frac{p\theta R^\alpha}{2\pi\sigma^2}\int_{B(y,\sqrt{2}\sigma)}\frac{1}{\|z\|^\alpha+\theta R^\alpha}\mathrm{d}z}-1\right)\mathrm{d}y\right)\\
&\overset{(b)}{\leqslant}\frac{1}{p}\exp\left(\frac{2\lambda_0\pi\sigma^2 p\gamma R^2}{2\pi\sigma^2-p\gamma R^2}\right), \qquad \sigma > R\sqrt{\frac{p\gamma}{2\pi}},
\end{aligned} \tag{4.17}$$

where (a) holds since the non-negative function $1/\left(\|x\|^\alpha+\theta\right)$ is monotonically decreasing with the increase of $\|x\|$, the fact that the indicator function $\mathbf{1}(\|x\| \leqslant \sqrt{2}\sigma) \geqslant \exp\left(-\|x\|^2/2\sigma^2\right)$ for $\forall x \in B(0,\sqrt{2}\sigma)$, and

$$\int_{\mathbb{R}^2}\mathbf{1}(\|x\| \leqslant \sqrt{2}\sigma)\mathrm{d}x = \int_{\mathbb{R}^2}\exp(-\|x\|^2/2\sigma^2)\mathrm{d}x;$$

(b) follows from the proof of (4.16). □

$D_0(\theta \mid R)$ is identical to [15, (23)] and always finite for any given R and θ, so is $D_v(\theta \mid R)$. When $a \leqslant R\beta^{-1}$ ($a = a_0$ under UM and $a = \sqrt{2}\sigma$ under NM), we use $D_0(\theta \mid R)$ (the static case) to bound the local delay. If $a > R\beta^{-1}$, a tighter upper bound is provided in (4.11).

Propositions 4.3 and 4.5 present generalized expressions of the conditional Laplace

transform of the interference I and the conditional local delay in mobile networks[4] given a transmission distance. (4.10) and (4.11) are corresponding lower and upper bounds, respectively, since the network realizations endure maximum temporal correlation in the static case and are mutually independent in the infinitely mobile case.

To demonstrate the impact of even a very low level of mobility, we calculate the slope of $D_v(\theta \mid R)$ at $a = 0$. Under UM, for example, the sensitivity of $D_v(\theta \mid R)$ at $a_0 = 0$ is given by

$$\left.\frac{\partial D_v(\theta \mid R)}{\partial a_0}\right|_{a_0=0} = -\infty.$$

This shows that the local delay decreases drastically with small excursions from the interferers since the uncertainty induced by mobility greatly reduces the temporal correlation of the interference. An identical result also holds for NM. Figure 4.2 shows the local delay as a function of the mean speed $\bar{v}$ under UM and NM. The simulation curves and upper bounds show the results for the intermediate mobility regime between the static case and the infinitely mobile case. Random mobility of the interferers positively affects the network performance (in terms of the local delay). Long local delays are due to the high temporal correlation of the interference and thus outage, and the random mobility reduces such correlation [56]. The more uncertainty the mobility induces, the less correlated the outage. Therefore, fewer transmission attempts are necessary. Both lower and upper bounds in (4.10) and (4.11) get tight as the mean speed $\bar{v}$ increases.

4.3.2 Block mobility

In the previous analysis we assumed fast mobility, where nodes update locations in every time slot. However, this may not be an appropriate assumption for all networks. In a heavy-traffic network, for example, a large number of packets are transferred

[4]Recall that mobility models only apply to interferers in this section.

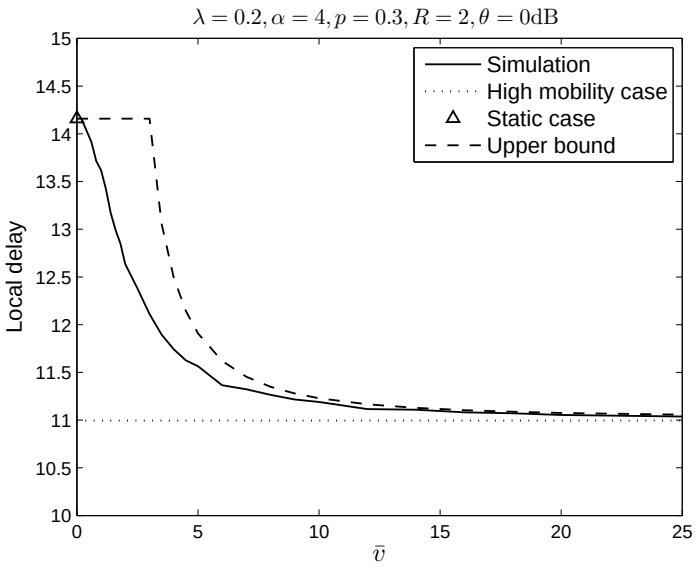

(a) UM case

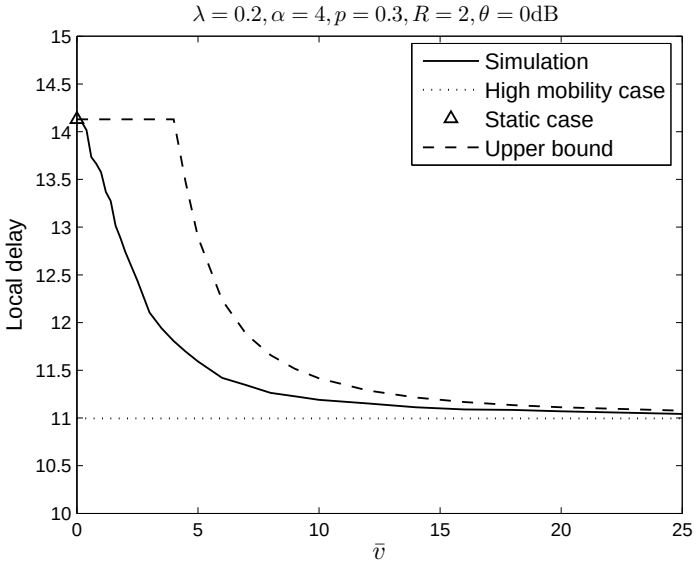

(b) NM case

Figure 4.2. The conditional local delay $D_v(\theta \mid R)$ as a function of the mean speed $\bar{v}$ under UM and NM. $\bar{v} = 128a_0/45\pi$ for UM and $\bar{v} = \sqrt{\pi}\sigma$ for NM. The simulation result is the solid curve. The dashed curve is an upper bound from (4.11). The dotted line is the infinitely mobile case, which provides a lower bound. The static case ($v = 0$) is represented in a triangle.

before a node makes a significant location change. Another example is a mobile network with low speed. In these cases, it is reasonable to use the block mobility model, which includes dwell slots. A node updates its location with probability $1/K$, where $K > 1$, and stays in its previous location with probability $1 - 1/K$. K is the *average location coherence time*. The multi-path fading component, however, is i.i.d. in different time slots. Again, slotted ALOHA is assumed as the MAC scheme.

For any time $t \in \mathbb{Z}$, we partition the transmitter process Φ_t into two PPPs,

$$\Phi_{t,1} = \{x_i(t) \in \Phi_t : x_i(t) \neq x_i(t-1)\}$$

and

$$\Phi_{t,2} = \{x_i(t) \in \Phi_t : x_i(t) = x_i(t-1)\}.$$

The nodes in $\Phi_{t,1}$ update their locations in time t while the nodes in $\Phi_{t,2}$ do not move. $\Phi_{t,1}$ and $\Phi_{t,2}$ are independent with intensities λ_0/K and $\lambda_0(K-1)/K$, respectively, due to the independent thinning of the PPP. The total interference is then given by

$$\begin{aligned} I(t) &= \sum_{x \in \Phi_{t,1}} T_x h_x \left\|x(t)\right\|^{-\alpha} + \sum_{x \in \Phi_{t,2}} T_x h_x \left\|x(t)\right\|^{-\alpha} \\ &= \sum_{y \in \tilde{\Phi}_1} T_y h_y \left\|y + w_y(t)\right\|^{-\alpha} + \sum_{x \in \Phi_{t,2}} T_x h_x \left\|x(t)\right\|^{-\alpha}, \end{aligned}$$

where $\tilde{\Phi}_1$ is the home location process of the nodes in $\Phi_{t,1}$. In this case, the static elements $\mathcal{S}$ in the network are $\mathcal{S} = \tilde{\Phi}_1 \cup \Phi_2$. We have the following corollary about the conditional Laplace transform of the interference I and the conditional local delay for a given R under the block mobility case.

Corollary 4.6. *Given the static elements of a network $\mathcal{S} = \tilde{\Phi}_1 \cup \Phi_2$, where $\tilde{\Phi}_1$ and Φ_2 are independent, the conditional Laplace transform of the interference $I(t)$ is given by*

$$\mathcal{L}_I(s \mid \mathcal{S}) = \mathcal{L}_v(s \mid \tilde{\Phi}_1)\mathcal{L}_0(s \mid \Phi_2), \tag{4.18}$$

where $\mathcal{L}_v(\cdot)$ and $\mathcal{L}_0(\cdot)$ are from (4.8) and (4.6), respectively. Let $a = a_0$ under UM and $a = \sqrt{2}\sigma$ under NM. Given the transmission distance R, the conditional local delay is upper bounded by

$$D_K(\theta \,|\, R) \leqslant \begin{cases} D_0(\theta \,|\, R) \cdot \exp\left(\frac{\lambda_0 p\gamma R^2}{K}\left(\frac{\pi a^2}{\pi a^2 - p\gamma R^2} - \frac{1}{q^{1-\delta}}\right)\right) & \\ & a\beta > R \\ D_0(\theta \mid R) & \text{otherwise,} \end{cases} \tag{4.19}$$

where the spatial contention γ is from (4.13), $\beta \triangleq \sqrt{(1-q^{1-\delta})\,\pi/p\gamma}$, and $D_0(\theta \mid R)$ is from (4.12).

Proof. $\mathcal{L}_I(s \mid \mathcal{S})$ in (4.18) is straightforward due to the independence property of $\tilde{\Phi}_1$ and Φ_2. For the local delay, we have

$$D_K(\theta \,|\, R) = \frac{1}{p}\mathbb{E}_{\tilde{\Phi}_1}\left(\frac{1}{\mathcal{L}_I(s \mid \tilde{\Phi}_1)}\right)\mathbb{E}_{\Phi_2}\left(\frac{1}{\mathcal{L}_I(s \mid \Phi_2)}\right)\Bigg|_{s=\theta R^\alpha}.$$

The rest of the steps follow the proofs of (4.9) and (4.11) in Propositions 4.3 and 4.5, respectively. □

Figure 4.3 shows the local delay as a function of the mean location coherence time K under both UM and NM. The mean speed in the simulations is set at $\bar{v} = 7/K$. The mean speed decreases with the increase of the mean coherence time K, since the average hop length of nodes (if the node moves) is kept constant. The mean coherence time K greatly affects the local delay in the low K regime, while its impact shrinks in the high K regime. (4.19) provides a tight upper bound and thus can be used to approximate the intermediate results between the static and fast mobility cases. For the case where the dwell time is a constant, the local delay can be analyzed through similar steps.

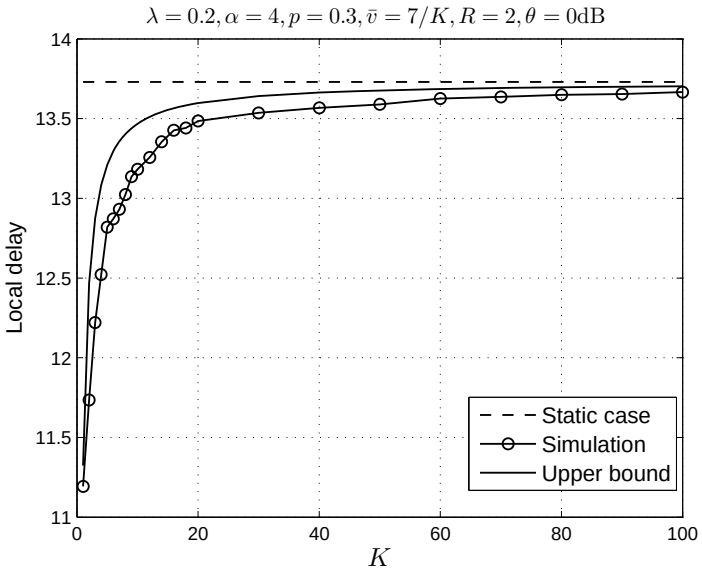

(a) UM case

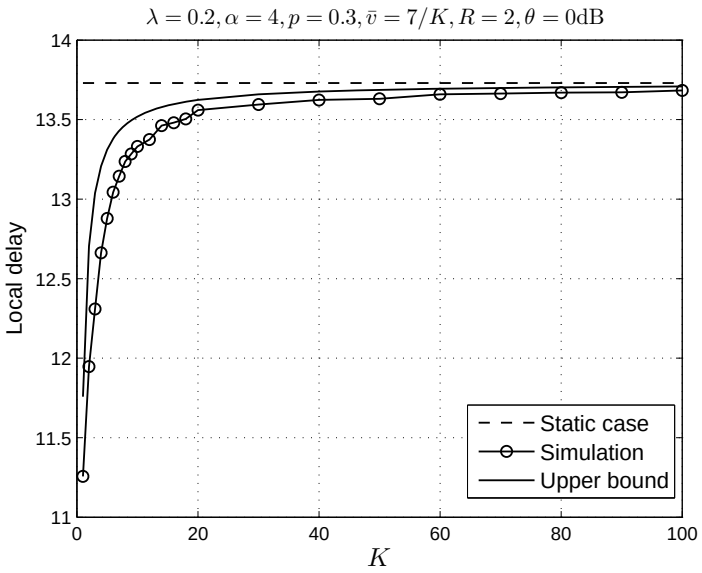

(b) NM case

Figure 4.3. The conditional local delay $D_K(\theta \mid R)$ as a function of the mean location coherence time K under UM and NM. The simulation and an upper bound from (4.19) are marked by circles and solid curve, respectively. The dashed line is the static case.

4.4 Local delay for random static transmission distance

In the previous section, we evaluated the local delay for a given transmission distance R. If R itself is a random variable, we can average over the random distance by

$$D_v = \mathbb{E}_R \left[D_v \left(\theta \mid R \right) \right].$$

Note that we still do not consider mobility in the desired link (mobility models only apply to the interferers). The randomness of R is due to the spatial averaging over different network realizations. In the rest of the chapter, we assume fast mobility at the interferers. Block mobility ($K > 1$) can be treated similarly by replacing $D_v(\theta \mid R)$ by $D_K(\theta \mid R)$. As already defined in Section 4.2.4, the desired receiver is located at the origin o. If the location of the desired transmitter is uniformly distributed, we have the following proposition about the local delay.

Proposition 4.7. *Assume that the desired transmitter is uniformly distributed around o with radius a_0 so that R is distributed as given in (4.2), and the interferers follow UM. The local delay for $\beta = \sqrt{(1-q^{1-\delta})\,\pi/p\gamma} < 1$ is upper bounded by*

$$\begin{aligned} D_{\mathrm{FMOI},a_0} \;\leqslant\; & \frac{\pi}{\gamma p^2}\left(1 - q^{1-\delta} e^{\bar{c}_u\left(q^{\delta-1}-1\right)}\right) + \\ & \frac{\pi \bar{c}_u e^{-\bar{c}_u}}{\gamma p^2}\left(\mathrm{Ei}\left(\bar{c}_u q^{\delta-1}\right) - \mathrm{Ei}(\bar{c}_u)\right) + \\ & \frac{\pi q^{1-\delta}}{\gamma \bar{c}_u p^2}\left(e^{\frac{\bar{c}_u p\gamma}{\pi q^{1-\delta}}} - e^{\bar{c}_u\left(q^{\delta-1}-1\right)}\right), \end{aligned} \tag{4.20}$$

where $\mathrm{Ei}(x) \triangleq \int_{-\infty}^{x} t^{-1} e^t \mathrm{d}t$, $\bar{c}_u \triangleq \lambda_0 \pi a_0^2$ *is the mean number of nodes in a circular region of radius a_0, and "*FMOI*" is the abbreviation of "fast mobility only at interferers".*

For $\beta \geqslant 1$, the local delay is upper bounded by

$$D_{\mathrm{FMOI},a_0} \leqslant \frac{\pi}{\gamma p^2}\left(1-(1-\frac{p\gamma}{\pi})e^{\frac{\bar{c}_u p\gamma}{\pi-p\gamma}}+ \bar{c}_u e^{-\bar{c}_u}\left(\mathrm{Ei}\left(\frac{\pi\bar{c}_u}{\pi-p\gamma}\right)-\mathrm{Ei}(\bar{c}_u)\right)\right). \tag{4.21}$$

The local delay is lower bounded by

$$D_{\mathrm{FMOI},a_0} \geqslant \frac{\pi}{\gamma\bar{c}_u p^2}\left(e^{\frac{\bar{c}_u p\gamma}{\pi}}-1\right). \tag{4.22}$$

Proof. For a given transmission distance R, an upper bound of the conditional local delay $D_v(\theta \mid R)$ is given in (4.11). If the location of the desired transmitter is uniformly distributed, we obtain

$$\begin{aligned} D_{\mathrm{FMOI},a_0} &\leqslant \int_0^{a_0} f_R(r) D_v(\theta \mid r)\mathrm{d}r \\ &= \begin{cases} \frac{1}{pa_0^2}\int_0^{\beta^2 a_0^2}\exp\left(\frac{\bar{c}_u x}{\pi a_0^2-p\gamma x}\right)\mathrm{d}x+ & \\ \frac{1}{a_0^2}\int_{\beta a_0}^{a_0} 2x D_0(\theta x^\alpha)\mathrm{d}x & \beta<1 \\ \frac{1}{pa_0^2}\int_0^{a_0^2}\exp\left(\frac{\bar{c}_u x}{\pi a_0^2-p\gamma x}\right)\mathrm{d}x & \beta\geqslant 1, \end{cases} \end{aligned}$$

where $f_R(r)$ is from (4.2). On the other hand,

$$D_{\mathrm{FMOI},a_0} \geqslant \int_0^{a_0} f_R(r) D_\infty(\theta \mid r)\mathrm{d}r,$$

where $D_\infty(\theta \mid r)$ is from (4.10). The rest of the steps are straightforward. □

Similarly we have the following proposition, if the location of the desired transmitter is normally distributed.

Proposition 4.8. *Assume that the desired transmitter is normally distributed around*

o with parameter σ so that the distribution of R is given in (4.4), and the interferers follow NM. Let $\beta = \sqrt{(1-q^{1-\delta})\pi/p\gamma}$. The local delay is upper bounded by

$$\begin{aligned} D_{\mathrm{FMOI},\sigma} \;<\; & \frac{\pi}{\gamma p^2} \exp\left(\left(q^{1-\delta}-1\right)\left(\frac{\pi}{p\gamma} - \bar{c}_n q^{\delta-1}\right)\right) \cdot \\ & \left(1 - q^{1-\delta} + \frac{p\gamma}{\pi - p\gamma\bar{c}_n q^{\delta-1}}\right), \end{aligned} \tag{4.23}$$

if $2\sigma^2 < q^{1-\delta}/\lambda_0 p\gamma$, where $\bar{c}_n \triangleq 2\lambda_0\pi\sigma^2$, and lower bounded by

$$D_{\mathrm{FMOI},\sigma} \geqslant \frac{\pi}{p\left(\pi - \bar{c}_n p\gamma\right)}, \tag{4.24}$$

if $2\sigma^2 < 1/\lambda_0 p\gamma$. The local delay is infinite for $2\sigma^2 > q^{1-\delta}/\lambda_0 p\gamma$.

Proof. Similar to the proof of Proposition 4.7, the local delay is lower bounded by

$$D_{\mathrm{FMOI},\sigma} \geqslant \int_0^\infty \frac{1}{2\sigma^2 p} \exp\left(-\frac{x}{2\sigma^2} + \lambda_0 p\gamma x\right) \mathrm{d}x.$$

The integral is bounded if $2\sigma^2 < 1/\lambda_0 p\gamma$. On the other hand, the local delay is upper bounded by

$$\begin{aligned} & D_{\mathrm{FMOI},\sigma} \\ & \leqslant \int_0^{2\beta^2\sigma^2} \frac{1}{2\sigma^2 p} \exp\left(-\frac{x}{2\sigma^2} + \frac{\bar{c}_n p\gamma x}{2\pi\sigma^2 - p\gamma x}\right) \mathrm{d}x + \\ & \quad \int_{2\beta^2\sigma^2}^\infty \frac{1}{2\sigma^2 p} \exp\left(-\frac{x}{2\sigma^2} + \frac{\lambda_0 p\gamma x}{q^{1-\delta}}\right) \mathrm{d}x \\ & \overset{(a)}{=} \frac{\pi \exp\left(\left(q^{1-\delta}-1\right)\left(\frac{\pi}{p\gamma} - \bar{c}_n q^{\delta-1}\right)\right)}{p\left(\pi - p\gamma\bar{c}_n q^{\delta-1}\right)} + \\ & \quad \frac{\exp(-\frac{\pi}{p\gamma} - \bar{c}_n)}{2\sigma^2 p} \int_{2\pi\sigma^2 q^{1-\delta}/p\gamma}^{2\pi\sigma^2/p\gamma} \exp\left(\frac{x}{2\sigma^2} + \frac{2\bar{c}_n\sigma^2\pi}{p\gamma x}\right) \mathrm{d}x, \end{aligned}$$

where (a) holds when $2\sigma^2 < q^{1-\delta}/\lambda_0 p\gamma$. For small σ, we obtain

$$\begin{aligned}\int_{2\pi\sigma^2 q^{1-\delta}/p\gamma}^{2\pi\sigma^2/p\gamma} \exp\left(\frac{x}{2\sigma^2} + \frac{2\pi\sigma^2\bar{c}_n}{p\gamma x}\right) \mathrm{d}x \\ \approx \quad \frac{2\pi\sigma^2}{p\gamma}\left(1-q^{1-\delta}\right)\exp\left(\frac{\pi q^{1-\delta}}{p\gamma} + \bar{c}_n q^{\delta-1}\right).\end{aligned}$$

□

The local delay is always finite if the location of the desired transmitter is uniformly distributed, since the support of transmission distance R is finite. Figure 4.4 corroborates the observation. This observation can be extended to any pdf of R via Proposition 4.5 as long as it has finite support. If the location of the desired transmitter is normally distributed, however, the local delay is finite only if $2\sigma^2 < q^{1-\delta}/\lambda_0 p\gamma$. If the randomness of the transmission distance induces too much uncertainty in the typical link, the local delay becomes heavy-tailed. The infinity of the local delay does not imply that a node can not convey a message to other nodes in the network in a finite time. However, it implies that the distribution of the local delay is heavy-tailed.

The next proposition contrasts the local delay for mobility only at interferers with the result for static networks.

Proposition 4.9. *If the location of the desired transmitter is uniformly distributed, the local delay in a static network is given by*

$$D_{\mathrm{static},a_0} = \frac{\pi q^{1-\delta}}{\bar{c}_u \gamma p^2}\left[\exp\left(\frac{\bar{c}_u p\gamma}{\pi q^{1-\delta}}\right) - 1\right]. \tag{4.25}$$

If the location of the desired transmitter is normally distributed, the local delay is finite if $2\sigma^2 < q^{1-\delta}/\lambda_0 p\gamma$ *and given by*

$$D_{\mathrm{static},\sigma} = \frac{\pi q^{1-\delta}}{p\left(\pi q^{1-\delta} - \bar{c}_n p\gamma\right)}. \tag{4.26}$$

Proof. In a static network, the static elements in the network are $\mathcal{S} = \Phi$. Given a transmission distance R, the local delay is given by $D_0(\theta \mid R)$, which is from (4.12). Deconditioning on the random variable R in (4.12) using (4.2), we have

$$D_{\text{static},a_0} = \int_0^{a_0} \frac{2r}{a_0^2} D_0(\theta \mid r) \mathrm{d}r,$$

which yields (4.25). Similarly for the Rayleigh pdf of R given in (4.4), we have

$$D_{\text{static},\sigma} = \int_0^{\infty} \frac{r}{p\sigma^2} \exp\left(\frac{\lambda_0 p\gamma r^2}{q^{1-\delta}} - \frac{r^2}{2\sigma^2}\right) \mathrm{d}r.$$

The integral is finite if $2\sigma^2 < q^{1-\delta}/\lambda_0 p\gamma$. (4.26) then follows from straightforward calculations. □

We denote by $\overline{D}_{\text{FMOI},a_0}$ and $\overline{D}_{\text{FMOI},\sigma}$ the upper bounds of the local delay given in Proposition 4.7 and 4.8, respectively. We then have the following corollary.

Corollary 4.10. *For $a_0 \to \infty$, $\overline{D}_{\text{FMOI},a_0}$ and D_{static,a_0} have the following relationship*

$$\overline{D}_{\text{FMOI},a_0} = \begin{cases} \Theta\left(D_{\text{static},a_0}\right) & \beta < 1 \\ o\left(D_{\text{static},a_0}\right) & \beta \geqslant 1. \end{cases} \tag{4.27}$$

For $\sigma = \sqrt{\frac{q^{1-\delta}}{2\lambda_0 p\gamma}}$, we have

$$\left.\frac{\overline{D}_{\text{FMOI},\sigma}}{D_{\text{static},\sigma}}\right|_{\sigma=\sqrt{\frac{q^{1-\delta}}{2\lambda_0 p\gamma}}} = 1. \tag{4.28}$$

Proof. Based on (4.25), it is straightforward to find that for $a_0 \to \infty$,

$$D_{\text{static},a_0} = \Theta\left(\frac{\exp\left(\frac{\bar{c}_u p\gamma}{\pi q^{1-\delta}}\right)}{\bar{c}_u}\right).$$

For $\beta < 1$, $\overline{D}_{\text{FMOI}}$ is given in (4.20). We have

$$\lim_{a_0\to\infty}\frac{\overline{D}_{\text{FMOI},a_0}\bar{c}_u}{\exp\left(\frac{\bar{c}_u p\gamma}{\pi q^{1-\delta}}\right)} \overset{(a)}{=} \lim_{a\to\infty}\frac{\bar{c}_u^2\int_{\bar{c}_u}^{\bar{c}_u q^{\delta-1}}\exp(t)/t\mathrm{d}t}{\exp\left(\frac{\bar{c}_u(\pi q^{1-\delta}+p\gamma)}{\pi q^{1-\delta}}\right)} + \frac{\pi q^{1-\delta}}{\gamma p^2}$$
$$\overset{(b)}{=} \frac{\pi q^{1-\delta}}{\gamma p^2} < \infty,$$

where (a) and (b) hold due to L'Hopital's rule and the fact that the parameter $\beta = \sqrt{(1-q^{1-\delta})\pi/p\gamma} < 1$. Hence, we have

$$\overline{D}_{\text{FMOI},a_0} = \Theta\left(D_{\text{static},a_0}\right), \qquad \beta < 1.$$

For $\beta > 1$, on the other hand, $\overline{D}_{\text{FMOI}}$ is given in (4.21). It is straightforward to show that

$$\lim_{a_0\to\infty}\frac{\overline{D}_{\text{FMOI},a_0}\bar{c}_u}{\exp\left(\frac{p\gamma\bar{c}_u}{\pi q^{1-\delta}}\right)} = 0.$$

For $\beta = 1$, we have

$$\begin{aligned}
&\lim_{a_0\to\infty}\frac{\overline{D}_{\text{FMOI},a_0}\bar{c}_u}{\exp\left(\frac{\bar{c}_u p\gamma}{\pi q^{1-\delta}}\right)} \\
&\quad= \lim_{a_0\to\infty}\frac{\pi\bar{c}_u\int_{\bar{c}_u}^{\pi\bar{c}_u/(\pi-p\gamma)}\exp(t)/t\mathrm{d}t}{\gamma p^2\exp\left(\bar{c}_u(\pi q^{1-\delta}+p\gamma)/\pi q^{1-\delta}\right)} - \\
&\qquad\lim_{a_0\to\infty}\left(1-\frac{p\gamma}{\pi}\right)\frac{\pi\bar{c}_u}{\gamma p^2} \\
&\quad\overset{(a)}{=} 0,
\end{aligned}$$

where (a) holds due to the fact that $\pi - p\gamma = \pi q^{1-\delta}$. (4.27) is then proved.

For $\sigma = \sqrt{q^{1-\delta}/2\lambda_0 p\gamma}$, (4.28) is then immediate from (4.23) and (4.26) via L'Hopital's rule. □

We define $\bar{R} \triangleq \mathbb{E}[R]$ as the mean transmission distance. Figures 4.4 shows the local delay as a function of $\bar{R}$ for both $\beta < 1$ and $\beta \geqslant 1$. We find that mobility at

the interferers helps reduce the local delay. However, the local delay is dominantly affected by the distribution of the transmission distance.

4.5 Local delay for random time-variant transmission distance

In this section, we evaluate the local delay under several transmission schemes. Conditioned on $o \in \tilde{\Phi}$, the success probability given the static element $\mathcal{S}$ is given by

$$\mathbb{P}^o\left(\mathcal{C}_{\mathcal{S}}\right) = \mathbb{P}^o\left(\mathrm{SIR} > \theta \mid \mathcal{S}\right),$$

where $\mathbb{P}^o(\cdot)$ is the Palm distribution [4]. The local delay is then given by

$$D \triangleq \mathbb{E}^o_{\mathcal{S}}\left(\frac{1}{\mathbb{P}^o(\mathcal{C}_{\mathcal{S}})}\right).$$

4.5.1 Random bipolar model

Here, we evaluate the local delay under the random bipolar model, which is described in Section 4.2.2. It is complicated to analyze the case of fast mobility in both desired and interfering links directly. Hence we consider a joint random variable $G \triangleq hR^{-\alpha}$, since the macroscopic mobility in wireless networks can be treated as another source of uncertainty in addition to multipath fading [48, 56]. Given the static elements in the network $\mathcal{S} = \tilde{\Phi}$, the conditional success probability is

$$\mathbb{P}^o(G > \theta I(t) \mid \tilde{\Phi}) = \mathbb{E}_G\left[\mathbb{P}^o\left(I(t) < \theta^{-1}G \mid G, \tilde{\Phi}\right)\right].$$

In order to evaluate the local delay, we need the following lemma.

Lemma 4.11. *For a static network (the static elements in the network $\mathcal{S} = \Phi$), we*

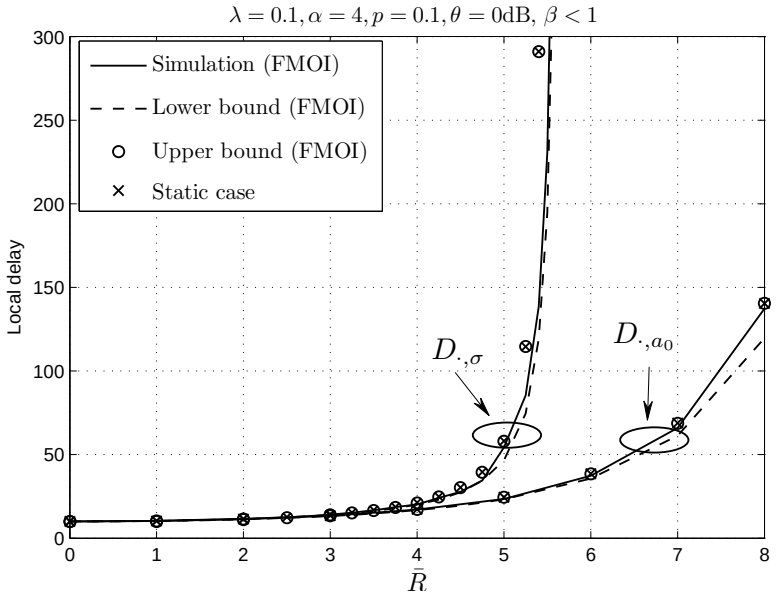

(a) $\beta < 1$

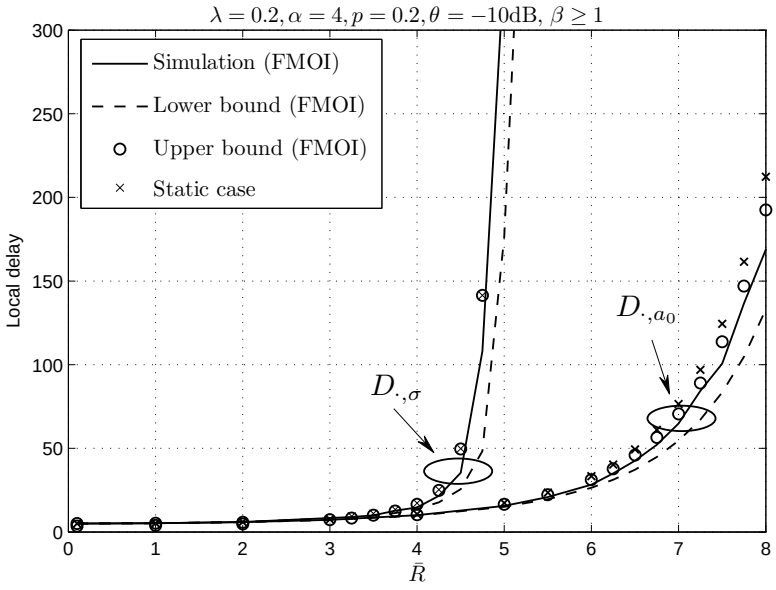

(b) $\beta \geqslant 1$

Figure 4.4. The local delay as a function of the mean transmission distance $\bar{R} = \mathbb{E}[R]$, where $a_0 = 45\pi\bar{R}/128$ and $\sigma = \bar{R}/\sqrt{\pi}$. The solid curve shows the simulation results for fast mobility only at interferers with their upper and lower bounds in circles and dashed lines, respectively. The crosses are the static case.

have the following relationship of the conditional success probability

$$\mathbb{E}_G\left[\mathbb{P}^o\left(I(t) < \theta^{-1}G \mid G, \Phi\right)\right] \geqslant \mathbb{P}^o\left(I(t) < \theta^{-1}\mathbb{E}[G] \mid \Phi\right). \tag{4.29}$$

Proof. We have

$$\begin{aligned}
&\frac{\partial^2}{\partial G^2}\mathbb{P}^o\left(I(t) < \theta^{-1}G \mid G, \Phi\right) \\
=&\frac{\partial^2}{\partial G^2}\prod_{x\in\Phi}\left(1 - \frac{p\theta^{-1}G}{\|x\|^\alpha + G\theta^{-1}}\right) \\
=&\frac{\partial}{\partial G}\sum_{x_i\in\Phi}\left(-\frac{p\theta^{-1}\|x_i\|^\alpha}{\left(\|x_i\|^\alpha + G\theta^{-1}\right)^2}\prod_{x\in\Phi, x\neq x_i}\left(1 - \frac{p\theta^{-1}G}{\|x\|^\alpha + G\theta^{-1}}\right)\right) \\
=&\sum_{x_i\in\Phi}\left(\frac{2p\theta^{-1}\|x_i\|^\alpha}{\left(\|x_i\|^\alpha + G\theta^{-1}\right)^3}\prod_{x\in\Phi, x\neq x_i}\left(1 - \frac{p\theta^{-1}G}{\|x\|^\alpha + G\theta^{-1}}\right)\right) + \\
&\sum_{x_i\in\Phi}\sum_{x_j\in\Phi, x_j\neq x_i}\left(\prod_{x\in\{x_i,x_j\}}\frac{p\theta^{-1}\|x\|^\alpha}{\left(\|x\|^\alpha + G\theta^{-1}\right)^2}\cdot\right. \\
&\left.\prod_{x\in\Phi\setminus\{x_i,x_j\}}\left(1 - \frac{p\theta^{-1}G}{\|x\|^\alpha + G\theta^{-1}}\right)\right) \\
\geqslant&0.
\end{aligned}$$

Hence (4.29) holds due to Jensen's inequality. □

Deconditioning on the point process leads to the following proposition.

Proposition 4.12. *The local delay under the random bipolar model is always finite, i.e.,*

$$D_v = \mathbb{E}^o_{\tilde{\Phi}}\left[\frac{1}{p\mathbb{E}_G\left[\mathbb{P}^o\left(I(t) < \theta^{-1}G \mid G, \tilde{\Phi}\right)\right]}\right] < \infty.$$

Proof. The local delay under the random bipolar model is given by

$$\begin{aligned}
&\mathbb{E}^o_{\tilde{\Phi}}\left[\frac{1}{p\mathbb{E}_G\left[\mathbb{P}^o\left(I(t)<\theta^{-1}G \mid G,\tilde{\Phi}\right)\right]}\right] \\
&\qquad \leqslant \quad \mathbb{E}^o_{\Phi}\left[\frac{1}{p\mathbb{E}_G\left[\mathbb{P}^o\left(I(t)<\theta^{-1}G \mid G,\Phi\right)\right]}\right] \\
&\qquad \overset{(a)}{\leqslant} \quad \mathbb{E}^o_{\Phi}\left[\frac{1}{p\mathbb{P}^o\left(I(t)<\theta^{-1}\mathbb{E}[G] \mid \Phi\right)}\right] \\
&\qquad < \quad \infty,
\end{aligned}$$

where (a) holds due to Lemma 4.11. □

The simulation results under the fast mobility case are shown in Figure 4.5. For comparison, we also show the conditional local delay for a given transmission distance R, where $R = 15\pi\bar{v}/64$, so that the mean transmission distance is at the identical level in different cases. The benefit of fast mobility is obvious from the figure, since the nodes take advantage of spatial diversity in the desired link and mobility reduces the temporal correlation of interference in the interfering links. We notice from the figures that the local delay increases with the mean speed $\bar{v}$. This is because the long transmission distance more than offsets the benefit of the spatial diversity of the desired transmitter. An alternative way is to let a transmitter talk to the receiver that is close to it, as explored in the next subsection.

4.5.2 Quasi-nearest-receiver (QNR) transmission

Here, we assume that each transmitter tries to talk to its quasi-nearest receiver whose home location is the closest to the receiver. We only discuss UM. Recall from Section 4.2.2.2 that the potential receiver process Ψ is a PPP with intensity $\lambda' = q\lambda_0$. The assumption maintains the same density of receivers as the nodes that are not scheduled for transmission. Ψ is independent of the transmitter process Φ_t. We assume the typical transmitter has its home location at the origin o and denote by

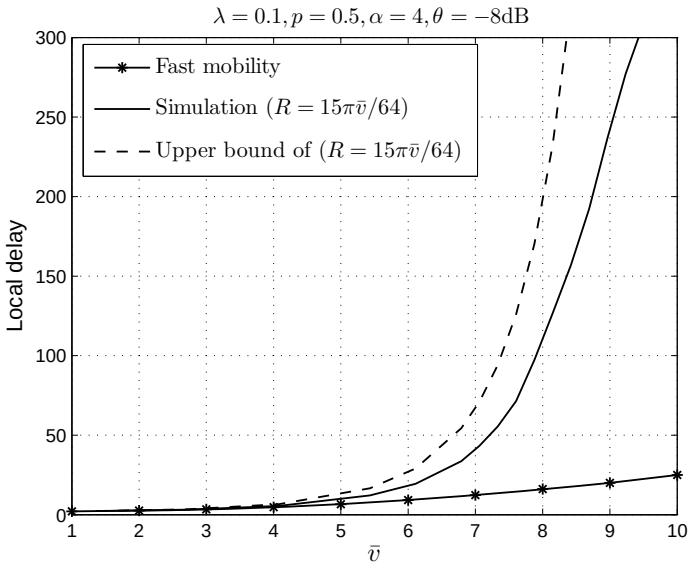

(a) UM case

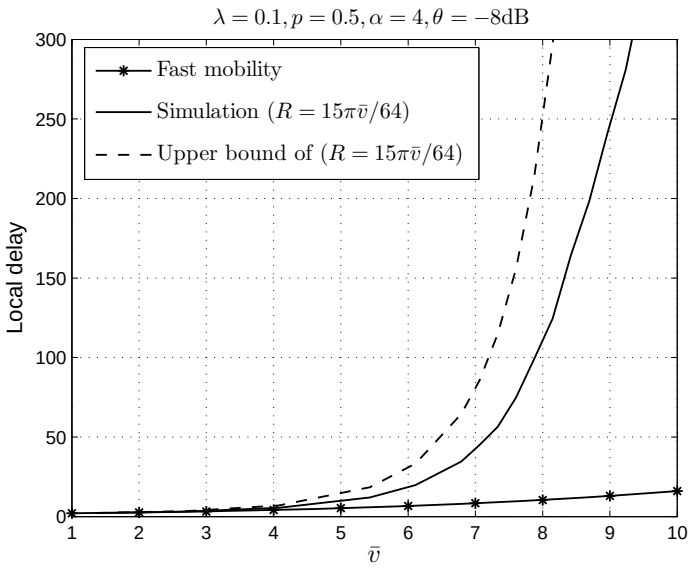

(b) NM case

Figure 4.5. Local delay under the random bipolar model for UM and NM. For comparison, the conditional local delay for a fixed transmission distance $R = 15\pi\bar{v}/64$ is also included, where the upper bound is from (4.11) with $R = 15\pi\bar{v}/64$.

R_0 the distance between the home location of the transmitter to its quasi-nearest receiver. To calculate the local delay under the quasi-nearest-receiver transmission, we need the following lemma.

Lemma 4.13. *Let R_0 denote the distance between the home location of the typical transmitter to its quasi-nearest receiver and a_0 denote the radius of the mobility region of the transmitter. Given R_0, upper and lower bounds of the local delay under the quasi-nearest-receiver transmission are given by $D_v(r_{\max})$ and $D_\infty(r_{\min})$, where $r_{\max} = R_0 + a_0$ and $r_{\min} = \max\{0, R_0 - a_0\}$.*

Proof. The lemma is proved by evaluating the local delay at two extreme points in the mobility region. □

Based on the Rayleigh distribution of R_0 obtained in [60], we have the following proposition.

Proposition 4.14. *A lower bound of the local delay under quasi-nearest-receiver transmission is given by*

$$\begin{aligned} \underline{D}_{\mathrm{QNR}} &= \frac{1}{p}\left(1 - e^{-q\bar{c}_u}\right) - \frac{2\pi q\lambda_0}{p}\exp\left(\frac{pq\gamma\bar{c}_u}{q\pi - p\gamma}\right)\cdot \\ &\quad \phi\left(a_0, \frac{a_0 p\gamma}{q\pi - p\gamma}, \frac{p\gamma - q\pi}{\pi}\right), \end{aligned} \tag{4.30}$$

if $p < \pi/(\pi + \gamma)$, where

$$\begin{aligned} \phi(x, m, s) &= \int_x^\infty t\exp\left(s(t+m)^2\right)\mathrm{d}t, \\ &= m\sqrt{\frac{\pi}{-s}}\left(\frac{1}{2}\mathrm{erf}\left(\frac{x}{\sqrt{2\sigma^2}} - \frac{1}{2}\right)\right) - \\ &\quad \frac{1}{2s}\exp\left(s\left(x+m\right)^2\right), \qquad s < 0. \end{aligned} \tag{4.31}$$

For $\beta \leqslant 1$, an upper bound of the local delay is given by

$$\overline{D}_{\mathrm{QNR}} = \frac{2\pi q\lambda_0}{p}\exp\left(\frac{pq\gamma\bar{c}_u}{q^{2-\delta}\pi - p\gamma}\right)\cdot \phi\left(0, \frac{p\gamma a_0}{p\gamma - q^{2-\delta}\pi}, \frac{\lambda_0\left(p\gamma - q^{2-\delta}\pi\right)}{q^{1-\delta}}\right), \tag{4.32}$$

if $q^{2-\delta}/p > \gamma/\pi$, where $\phi(x, m, s)$ is from (4.31).

For $\beta > 1$, we have an upper bound

$$\begin{aligned}\overline{D}_{\mathrm{QNR}} = &\frac{1}{p}\int_0^{(\beta-1)a_0}\varphi(x)\mathrm{d}x + \\ &\frac{2\pi q\lambda_0}{p}\exp\left(\frac{pq\gamma\bar{c}_u}{q^{2-\delta}\pi - p\gamma}\right)\cdot \\ &\phi\left((\beta-1)a_0, \frac{p\gamma a_0}{p\gamma - q^{2-\delta}\pi}\frac{\lambda_0\left(p\gamma - q^{2-\delta}\pi\right)}{q^{1-\delta}}\right),\end{aligned} \tag{4.33}$$

if $q^{2-\delta}/p > \gamma/\pi$, where

$$\varphi(x) = f_{R_0}(x)\exp\left(\frac{p\gamma\bar{c}_u(x+a_0)^2}{a_0^2\pi - p\gamma(x+a_0)^2}\right) \tag{4.34}$$

and $f_{R_0}(x) = 2\pi q\lambda_0 x e^{-\pi q\lambda_0 x^2}$.

Proof. From Lemma 4.13, a lower bound of the local delay is

$$\underline{D}_{\mathrm{QNR}} = \frac{1}{p}\int_0^{a_0} f_{R_0}(x)\mathrm{d}x + \int_{a_0}^{\infty} f_{R_0}(x)D_\infty(x-a_0)\mathrm{d}x.$$

The integral is finite if $p < \pi/(\pi+\gamma)$. On the other hand, an upper bound of the local delay is given by

$$\overline{D}_{\mathrm{QNR}} = \int_0^{\infty} f_{R_0}(x)D_v(x+a_0)\mathrm{d}x.$$

The integral is finite if $q^{2-\delta}/p > \gamma/\pi$. The rest of the calculation is straightforward. □

Figure 4.6 shows the local delay as a function of the MAC parameter p in mobile networks under quasi-nearest-receiver transmission. For comparison, the local delay in static networks is also included. From the figure, we observe that fast mobility reduces the local delay (compared to the static case), but it helps little to keep the local delay finite. This is due to the fact that the mobility induces limited diversity under the quasi-nearest-receiver transmission. For other transmission schemes such as quasi-nearest-neighbor transmission etc., we can calculate bounds of the local delay in similar ways.

4.5.3 Nearest-receiver (NR) transmission

If each transmitter always tries to talk its nearest receiver, we have the following proposition about the local delay.

Proposition 4.15. *The local delay under nearest-receiver transmission D_{NR} is lower and upper bounded by*

$$\underline{D}_{\mathrm{QNR}} \leqslant D_{\mathrm{NR}} \leqslant D_{\mathrm{QNR}}, \tag{4.35}$$

where $\underline{D}_{\mathrm{QNR}}$ is from (4.30).

Proof. Conditioned on that the quasi-nearest receiver of the typical transmitter is at $(R_0, 0)$, there are no other receivers in the ball of $B(o, R_0)$, where the origin o is the center of the ball and R_0 is the radius. Hence, even if the typical transmitter always chooses its nearest receiver, the transmission distance is not less than $r_{\min} = \max\{R_0 - a_0, 0\}$, where a_0 is the mobility radius of the transmitter. D_{NR} is then lower bounded by $\underline{D}_{\mathrm{QNR}}$. On the other hand, the typical transmitter changes the destination in different time t, if there is another receiver that is closer to the transmitter than the quasi-nearest receiver when the transmitter moves. The spatial

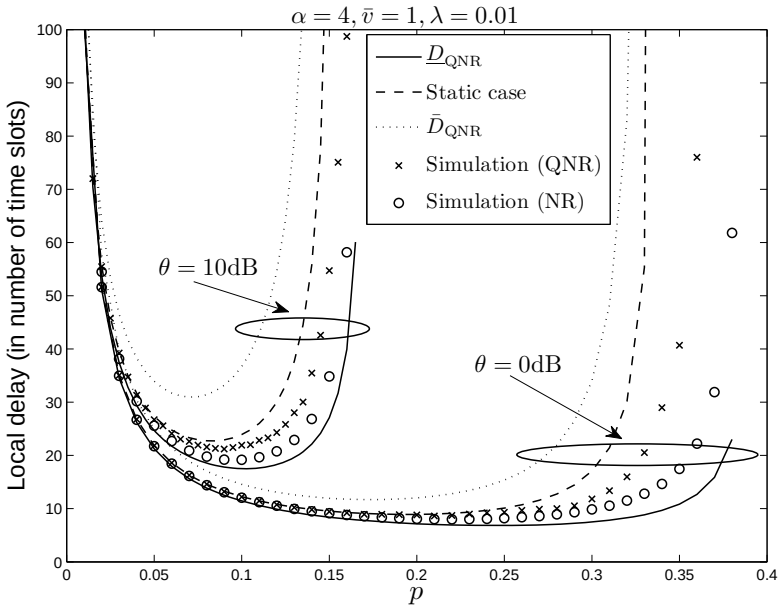

Figure 4.6. The local delay as a function of the transmission probability p under quasi-nearest-receiver and nearest-receiver transmission schemes. The crosses and circles are the simulation results of QNR and NR schemes, respectively. The dotted line is an upper bound of the local delay under the QNR scheme (see (4.32) and (4.33)). The dashed line is the static case. The solid curve is a lower bound of the local delay under the QNR scheme (see (4.30)).

correlation of the interference at different receivers is (much) lower. Hence, the local delay under nearest-receiver transmission is upper bounded by D_{QNR}. □

Figure 4.6 shows the simulation results of the local delay under nearest-receiver transmission, which corroborates Proposition 4.15.

4.6 Conclusions

In this chapter, we have evaluated the local delay in mobile Poisson networks for deterministic, random static, and random time-variant transmission distance. The results provide generalized expressions in addition to the two previously explored cases of static and infinitely mobile networks. Fast mobility has been shown to reduce the local delay in Poisson networks since the mobility of the interferers decreases the spatio-temporal correlation of the interference and outage, and mobility of the desired transmitter induces spatial diversity during transmission. The uniform and normal mobility models as specific examples lead to quantitively different local delay, even if the mean speeds of the nodes under two models are at an identical level. The range of network parameters under which a finite local delay can be achieved has also been derived, which depends on different mobility models and transmission schemes. Furthermore, the frequency with which the nodes make significant changes in locations greatly affects the local delay performance. The more frequently the nodes update their location, the fewer attempts a transmitter needs for packet transmission.

CHAPTER 5

SUMMARY AND FUTURE WORK

In this chapter, we summarize the theoretical work presented in previous chapters. We also list the contributions we have made in the experimental work, which is not included in this dissertation. Further, we discuss several possible directions for furture work from both theoretical and experimental aspects.

5.1 Summary of contributions

5.1.1 Theoretical results

This work focuses on the geometry analysis of mobile wireless networks. The theoretical contributions are summarized as follows.

- The fluctuations of the transmission distance in wireless networks have been characterized from fading perspective. Such large-scale fading, which is induced by macroscopic mobility, is viewed as another source of fading in wireless environments, in addition to the multi-path effects.

- The mean interference in a finite network has been calculated under different mobility models in Chapter 2. Several well-accepted mobility models have been separated into two categories: uniform and non-uniform. The mean interference at the center of a network under uniform mobility models is twice of the interference at the border. The mean interference at the center under the random waypoint model (as an example of non-uniform models) is asymptotically twice

the interference under uniform mobility models. For random waypoint, the interference at the border decreases to zero as the network radius goes large.

- A single-snapshot analysis of the network has been presented in Chapter 2 by evaluating the interference distribution and outage probability. The uniform mobility models do not affect the interference distribution compared to the static network. However the random waypoint mobility increases the interference at the origin and thus leads to higher outage probability. The nearest-interferer approximation has been applied to obtain a simple lower bound on the outage probability. Such lower bound is tight in low threshold regime.

- The temporal correlation of interference has been characterized in Chapter 3 in terms of the correlation coefficient of the interference. The more degrees of freedom the node explores, the faster the correlation coefficient decays with the mobility ranges. Multi-path fading and random MAC schemes have been shown to reduce the interference correlation as well.

- The temporal correlation of outage has been characterized in Chapter 3 in terms of the conditional outage probability. Given that a link is in outage in a certain time slot, the outage event in any other time slot is positively correlated.

- The local delay in mobile Poisson networks for deterministic, random static, and random time-variant transmission distance has been calculated in Chapter 4, which provides generalized expressions in addition to the two extreme cases: static and infinitely mobile networks. Mobility has been shown to reduce the local delay in Poisson network since the mobility of the desired transmitter induces spatial diversity and the mobility of the interferers decreases the correlation of the locations and thus the interference and outage.

5.1.2 Experimental results

This work focuses on the design and implementation of a software-defined radio system for superposition coding. The details can be found in [61, 62]. The experimental contributions are summarized as follows.

- A software-defined radio implementation of superposition coding has been proposed. A complete physical layer of the system has been designed on the GNU Radio / USRP platform.
- Sets of achievable rate-pairs (with different SNR conditions) under a packet error constraint have been experimentally determined. The results suggest that the superposition coding provides throughput gain over orthogonal schemes such as time division multiplexing.
- Our experimental findings question the validity of treating inter-user interference as Gaussian noise in theoretical analyses.

5.2 Future directions

By the theoretical and experimental results we have obtained, our work can be extended in several directions.

- As observed in Chapter 2 that the interference at the center of a finite network is larger than the interference at the border, the design of location-aware routing algorithms can be one of the research directions. We will try to explore when it is worthwhile routing traffic through the boundary nodes (with a longer routing path overall but less interference).
- Since the outage events are positively correlated (from Chapter 3), the design of correlation-aware retransmission schemes is necessary to more efficiently utilize

the network resource. If a link is in outage, several silence slots could be added rather than retransmit immediately since the conditional outage probability is higher. If fewer transmitters are concurrent, the success probability increases due to the decreased interference power.

- Superposition coding performance in mobile environment. In wireless communication, the user terminals are often mobile. As superposition coding is one of the possible solutions to increase the throughput, its performance results in mobile environment are not (yet) available, since mobility brings extra uncertainty in the channel estimation. Furthermore, the methods of grouping two users (receivers) in a network need to be explored. For vehicular communications, for example, the signal-to-noise ratios received at a vehicle (antennas assumed outside the vehicle) and at the user terminal inside the vehicle usually have several dB difference, which is reasonable environment for implementing superposition coding. The effectiveness and efficiency of the methods grouping two receivers need to be evaluated.

BIBLIOGRAPHY

1. D. Tse and P. Viswanath, *Fundamentals of Wireless Communication*. Cambridge University Press, 2005.

2. M. Haenggi, J. G. Andrews, F. Baccelli, O. Dousse, and M. Franceschetti, "Stochastic Geometry and Random Graphs for the Analysis and Design of Wireless Networks," *IEEE Journal on Selected Areas in Communications*, vol. 27, pp. 1029–1046, Sept. 2009.

3. F. Baccelli, *Stochastic Geometry and Wireless Networks. Volume II-Applications*. Foundations and Trends in Networking (NOW Publishers), vol. 4, no. 1-2, pp. 1-312, 2009.

4. M. Haenggi, *Stochastic Geometry for Wireless Networks*. Cambridge University Press, 2012.

5. R. M. Metcalfe and D. R. Boggs, "Ethernet: Distributed Packet Switching for Local Computer Networks," *Communications of the ACM*, vol. 19, no. 7, pp. 395–404, 1976.

6. D. Lipke, D. Swearingen, J. Parker, E. Steinbrecher, T. Calvit, and H. Dodel, "Marisat-A Maritime Satellite Communications System," *COMSAT Technical Review*, vol. 7, pp. 351–391, 1977.

7. B. Stavenow, "Throughput-Delay Characteristics and Stability Considerations of the Access Channel in a Mobile Telephone System," *ACM SIGMETRICS Performance Evaluation Review*, vol. 12, no. 3, pp. 105–112, 1984.

8. L. Kleinrock and F. Tobagi, "Packet Switching in Radio Channels: Part I–Carrier Sense Multiple-Access Modes and Their Throughput-Delay Characteristics," *IEEE Transactions on Communications*, vol. 23, no. 12, pp. 1400–1416, 1975.

9. M. Oliver and A. Escudero, "Study of Different CSMA/CA IEEE 802.11-Based Implementations," *Proceedings of EUNICE 1999 Contribution*, 1999.

10. D. Comer, *Computer Networks and Internets*. Pearson Prentice Hall, 2009.

11. M. Chiang, P. Hande, T. Lan, and C. W. Tan, *Power Control in Wireless Cellular Networks*. Foundations and Trends in Networking (NOW Publishers), vol. 2, no. 4, pp. 381-533 2009.

12. M. Haenggi and R. K. Ganti, *Interference in Large Wireless Networks*. Foundations and Trends in Networking (NOW Publishers), vol. 3, no. 2, pp. 127-248, 2009.

13. X. Zhang and M. Haenggi, "Random Power Control in Poisson Networks," *IEEE Transactions on Communications*, vol. 60, pp. 2602–2611, Sept. 2012.

14. F. Baccelli and B. Blaszczyszyn, "A New Phase Transition for Local Delays in MANETs," in *IEEE INFOCOM'10*, (San Diego, CA), Mar. 2010.

15. M. Haenggi, "The Local Delay in Poisson Networks," *IEEE Transactions on Information Theory*, vol. 59, pp. 1788–1802, Mar. 2013.

16. M. Penrose, *Random Geometric Graphs*. Oxford University Press, USA, 2003.

17. E. Sousa and J. Silvester, "Optimum Transmission Ranges in a Direct Sequence Spread-Spectrum Multihop Packet Radio Network," *IEEE Journal on Selected Areas in Communications*, vol. 8, pp. 762–771, Jun 1990.

18. E. Sousa, "Interference Modeling in a Direct-Sequence Spread-Spectrum Packet Radio Network," *IEEE Transactions on Communications*, vol. 38, no. 9, pp. 1475–1482, 1992.

19. F. Baccelli, B. Blaszczyszyn, and P. Muhlethaler, "An ALOHA Protocol for Multihop Mobile Wireless Networks," *IEEE Transactions on Information Theory*, vol. 52, no. 2, pp. 421–436, 2006.

20. M. Zorzi and S. Pupolin, "Optimum Transmission Ranges in Multihop Packet Radio Networks in the Presence of Fading," *IEEE Transactions on Communications*, vol. 43, no. 7, pp. 2201–2205, 2002.

21. S. Srinivasa and M. Haenggi, "Distance Distributions in Finite Uniformly Random Networks: Theory and Applications," *IEEE Transactions on Vehicular Technology*, vol. 59, pp. 940–949, Feb. 2010.

22. R. K. Ganti and M. Haenggi, "Interference and Outage in Clustered Wireless Ad Hoc Networks," *IEEE Transactions on Information Theory*, vol. 55, pp. 4067–4086, Sept. 2009.

23. R. K. Ganti and M. Haenggi, "Interference in Ad Hoc Networks with General Motion-Invariant Node Distributions," in *2008 IEEE International Symposium on Information Theory (ISIT'08)*, (Toronto, Canada), July 2008.

24. R. Giacomelli, R. K. Ganti, and M. Haenggi, "Outage Probability of General Ad Hoc Networks in the High-Reliability Regime," *IEEE/ACM Transactions on Networking*, vol. 19, pp. 1151–1163, Aug. 2011.

25. R. K. Ganti, J. G. Andrews, and M. Haenggi, "High-SIR Transmission Capacity of Wireless Networks with General Fading and Node Distribution," *IEEE Transactions on Information Theory*, vol. 57, pp. 3100–3116, May 2011.

26. C.-H. Lee and M. Haenggi, "Interference and Outage in Poisson Cognitive Networks," *IEEE Transactions on Wireless Communications*, vol. 11, pp. 1392–1401, Apr. 2012.

27. H. Nguyen, F. Baccelli, and D. Kofman, "A Stochastic Geometry Analysis of Dense IEEE 802.11 Networks," in *IEEE INFOCOM*, pp. 1199–1207, 2007.

28. O. Dousse, M. Franceschetti, and P. Thiran, "On the Throughput Scaling of Wireless Relay Networks," *IEEE/ACM Transactions on Networking*, vol. 14, no. 6, pp. 2756–2761, 2006.

29. R. K. Ganti and M. Haenggi, "Spatial Analysis of Opportunistic Downlink Relaying in a Two-Hop Cellular System," *IEEE Transactions on Communications*, vol. 60, pp. 1443–1450, May 2012.

30. F. Baccelli and C. Bordenave, "The Radial Spanning Tree of a Poisson Point Process," *Annals of Applied Probability*, vol. 17, no. 1, pp. 305–359, 2007.

31. M. Haenggi, "On Routing in Random Rayleigh Fading Networks," *IEEE Transactions on Wireless Communications*, vol. 4, pp. 1553–1562, July 2005.

32. F. Baccelli, B. Blaszczyszyn, and P. Muhlethaler, "On the Performance of Time-Space Opportunistic Routing in Multihop Mobile Ad Hoc Networks," in *7th International Symposium on Modeling and Optimization in Mobile, Ad Hoc, and Wireless Networks (WiOpt'09)*, Berlin, 2008.

33. S. P. Weber, X. Yang, J. G. Andrews, and G. D. Veciana, "Transmission Capacity of Wireless Ad Hoc Networks with Outage Constraints," *IEEE Transactions on Information Theory*, vol. 51, no. 12, pp. 4091–4102, 2005.

34. M. Haenggi, "Outage, Local Throughput, and Capacity of Random Wireless Networks," *IEEE Transactions on Wireless Communications*, vol. 8, pp. 4350–4359, Aug 2009.

35. R. K. Ganti and M. Haenggi, "Limit of the Transport Capacity of a Dense Wireless Network," *Journal of Applied Probability*, vol. 47, pp. 886–892, Sept. 2010.

36. R. K. Ganti and M. Haenggi, "Spatial and Temporal Correlation of the Interference in ALOHA Ad Hoc Networks," *IEEE Communications Letters*, vol. 13, no. 9, pp. 631–633, 2009.

37. R. K. Ganti and J. G. Andrews, "Correlation of Link Outage in Low-Mobility Spatial Wireless Networks," in *Asilomar Conference on Signals, Systems, and Computers*, (Pacific Grove), Nov. 2010.

38. U. Schilcher, G. Brandner, and C. Bettstetter, "Temporal Correlation of the Interference in Wireless Networks with Rayleigh Block Fading," *IEEE Transactions on Mobile Computing*, vol. 11, pp. 2109–2120, Dec. 2012.

39. M. Haenggi, "Diversity Loss due to Interference Correlation," *IEEE Communications Letters*, vol. 16, pp. 1600–1603, Oct. 2012.

40. Z. Kong and E. M. Yeh, "On the Latency for Information Dissemination in Mobile Wireless Networks," in *Proceedings of the 9th ACM International Symposium on Mobile Ad Hoc Networking and Computing (MobiHoc)*, Hong Kong SAR, China, May 2008.

41. M. Grossglauser and D. N. C. Tse, "Mobility Increases the Capacity of Ad Hoc Wireless Networks," *IEEE/ACM Transactions on Networking*, vol. 10, no. 4, pp. 477–486, 2002.

42. T. Camp, J. Boleng, and V. Davies, "A Survey of Mobility Models for Ad Hoc Network Research," *Wireless Communications and Mobile Computing*, vol. 2, no. 5, pp. 483–502, 2002.

43. S. Bandyopadhyay, E. J. Coyle, and T. Falck, "Stochastic Properties of Mobility Models in Mobile Ad Hoc Networks," *IEEE Transactions on Mobile Computing*, vol. 6, no. 11, pp. 1218–1229, 2007.

44. C. Bettstetter, "Mobility Modeling in Wireless Networks: Categorization, Smooth Movement, and Border Effects," *ACM SIGMOBILE Mobile Computing and Communications Review*, vol. 5, no. 3, p. 66, 2001.

45. C. Bettstetter, G. Resta, and P. Santi, "The Node Distribution of the Random Waypoint Mobility Model for Wireless Ad Hoc Networks," *IEEE Transactions on Mobile Computing*, vol. 2, no. 3, pp. 257–269, 2003.

46. C. Bettstetter, "On the Connectivity of Ad Hoc Networks," *The Computer Journal*, vol. 47, no. 4, p. 432, 2004.

47. E. Hyytia, P. Lassila, and J. Virtamo, "Spatial Node Distribution of the Random Waypoint Mobility Model with Applications," *IEEE Transactions on Mobile Computing*, vol. 5, no. 6, pp. 680–694, 2006.

48. M. Haenggi, "A Geometric Interpretation of Fading in Wireless Networks: Theory and Applications," *IEEE Transactions on Information Theory*, vol. 54, pp. 5500–5510, Dec 2008.

49. G. Alfano, R. Tresch, and M. Guillaud, "Spatial Diversity Impact on the Local Delay of Homogeneous and Clustered Wireless Networks," in *Smart Antennas (WSA), 2011 International ITG Workshop on*, pp. 1–6, IEEE, 2011.

50. K. Gulati, R. K. Ganti, J. G. Andrews, B. L. Evans, and S. Srikanteswara, "Characterizing Decentralized Wireless Networks with Temporal Correlation in the Low Outage Regime," *IEEE Transactions on Wireless Communications*, vol. 11, pp. 3112–3125, Aug. 2012.

51. M. J. Neely and E. Modiano, "Capacity and Delay Tradeoffs for Ad Hoc Mobile Networks," vol. 51, no. 6, pp. 1917–1937, 2005.

52. R. Vaze, "Throughput-Delay-Reliability Tradeoff with ARQ in Wireless Ad Hoc Networks," *IEEE Transactions on Wireless Communications*, vol. 10, no. 7, pp. 2142–2149, 2011.

53. M. J. Neely, "Optimal Energy and Delay Tradeoffs for Multi-User Wireless Downlinks," *IEEE Transcation on Information Theory*, vol. 53, pp. 3095–3113, Sept 2007.

54. J. Liu, X. Jiang, H. Nishiyama, and N. Kato, "Delay and Capacity in Ad Hoc Mobile Networks with F-cast Relay Algorithms," *IEEE Transactions on Wireless Communications*, vol. 10, no. 8, pp. 2738–2751, 2011.

55. L. Dai, "Stability and Delay Analysis of Buffered ALOHA Networks," *IEEE Transactions on Wireless Communications*, vol. 11, no. 8, pp. 2707–2719, 2012.

56. Z. Gong and M. Haenggi, "Interference and Outage in Mobile Random Networks: Expectation, Distribution, and Correlation," *IEEE Transactions on Mobile Computing*, Accepted, 2012. Available at `http://www.nd.edu/~mhaenggi/pubs/tmc13.pdf`.

57. Z. Gong and M. Haenggi, "The Local Delay in Mobile Poisson Networks," *IEEE Transactions on Wireless Communications*, 2013. Submitted.

58. P. Nain, D. Towsley, B. Liu, Z. Liu, and F. Inria, "Properties of Random Direction Models," in *IEEE INFOCOM*, vol. 3, 2005.

59. J. Kingman, "Uses of Exchangeability," *The Annals of Probability*, pp. 183–197, 1978.

60. M. Haenggi, "On Distances in Uniformly Random Networks," *IEEE Transactions on Information Theory*, vol. 51, pp. 3584–3586, Oct. 2005.

61. S. Vanka, S. Srinivasa, Z. Gong, P. Vizi, K. Stamatiou, and M. Haenggi, "Superposition Coding Strategies: Design and Experimental Evaluation," *IEEE Transactions on Wireless Communications*, vol. 11, pp. 2628–2639, Jul. 2012.

62. Z. Gong, S. Vanka, S. Srinivasa, P. Vizi, K. Stamatiou, and M. Haenggi, "Superposition Coding Strategies: Design and Experimental Evaluation," Tech. Rep. EWA2011-1, Emerging Wireless Architectures Laboratory, University of Notre Dame, Sept. 2011. Available at `http://www.nd.edu/~mhaenggi/pubs/techreport_sc11.pdf`.